A Computational Geometry Framework for Efficient Network Localization

Wenhan Dai, *Student Member, IEEE*, Yuan Shen, *Member, IEEE*, and Moe Z. Win, *Fellow, IEEE*

Abstract—Network localization is an emerging paradigm for providing high-accuracy positional information in GPS-challenged environments. To enable efficient network localization, we propose node prioritization strategies for allocating transmission resources among network nodes. This paper develops a computational geometry framework for determining the optimal node prioritization strategy. The framework consists of transforming each node prioritization strategy into a point in a Euclidian space and exploiting geometric properties of these points. Under this framework, we prove the sparsity property of the optimal node prioritization vector (NPV) and reduce the search space of the optimal NPV. Our approach yields exact optimal solutions rather than ϵ-approximate solutions for efficient network localization. Numerical results show that the proposed approach can significantly reduce the computational complexity of prioritization strategies and improve the accuracy of network localization.

Index Terms—Computational geometry, localization, sparsity, wireless networks.

I. INTRODUCTION

NETWORK LOCALIZATION is a promising paradigm for providing high-accuracy positional information in GPS-challenged scenarios [1]–[11]. Such information is crucial for many location-based applications, including autonomous logistics, building security, as well as search-and-rescue [8]–[16]. In network localization, there are two types of nodes, referred to as anchors and agents. The former have known positions and the latter have unknown positions. The position of an agent can be inferred from range measurements based on wireless signals transmitted by neighboring anchors (see Fig. 1).
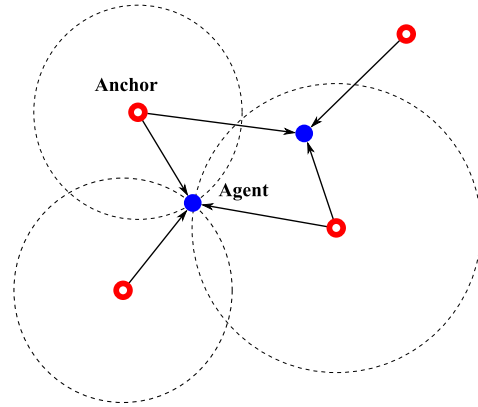
Fig. 1. Network localization scenario: agents (blue dots) determine their positions based on range measurements with respect to anchors (red circles).

The performance of network localization depends on various factors, such as transmission power, signal bandwidth, network geometry,[1] and propagation conditions [8]–[10], [17]–[20]. Among them, the allocation of transmission resources (e.g., power and bandwidth) plays a critical role since it not only affects network lifetime and throughput, but also determines the localization performance. For example, range measurements with anchors that give rise to poor network geometry can consume a significant amount of energy while providing diminishing localization accuracy improvement. Thus, it is essential to design node prioritization strategies for allocating transmission resources so that the best tradeoff between resource consumption and localization accuracy can be achieved [21], [22].

Extensive work has been carried out on maximizing communication and networking performance subject to resource constraints [23]–[26]. However, strategies designed for data networks are not suitable for localization networks since the performance metrics are different. In particular, a critical difference is that the performance metric in communication networks does not fully consider network geometry. Therefore, node prioritization calls for new formulations that account for the structure of the localization performance metric [27]–[30]. Two fundamental questions related to node prioritization are as follows:

1) How does localization performance depend on node prioritization strategies?
2) How can network nodes be prioritized for optimally allocating transmission resources?

[1]Network geometry refers to the relative positions among nodes in a localization network.

The answers to these questions will reveal the essence of node prioritization and guide the design of prioritization strategies for efficient network localization.

Current studies on efficient network localization [29]–[33] adopt certain functions of the Fisher information matrix (FIM) as the performance metrics. Typical functions include the trace of the inverted FIM [29]–[32], and the smaller eigenvalue of the FIM [32], [33]. These studies typically optimize the performance metric for given resource constraints using standard optimization programs. In [31], the problem of allocating transmission power for target localization is investigated, where the authors employed a relaxation method and obtained suboptimal solutions. In [32], the trace of the inverted FIM and the smaller eigenvalue of the FIM are shown as convex functions of the transmission power, and the corresponding power optimization problems for network localization are converted to conic programs. In [33], the ranging energy optimization problem for sensor positioning networks is formulated and a practical algorithm is proposed based on semi-definite programs (SDPs). Recent work [29] unifies the power optimization problem for active and passive localization and shows that the problem can be transformed into a second-order cone program (SOCP). All these approaches obtain ϵ-approximate solutions and rely on standard optimization engines [34], [35].

In this paper, we establish a computational geometry framework for node prioritization, aiming to achieve the optimal localization performance under resource constraints. We uncover an essential property, namely low-dimensionality of the localization performance metric. Such a property enables a linear transformation that maps each node prioritization strategy into a point in a three-dimensional Euclidian space. We determine several geometric properties based on this transformation and derive the optimal node prioritization strategies by exploiting these properties. The key contributions of this paper are as follows:

- We establish a computational geometry framework for node prioritization, exploiting the low-dimensionality of the performance metric;
- We determine the sparsity property of the optimal node prioritization vector (NPV), i.e., the optimal localization performance can be achieved by allocating resources to only a small subset of anchors;
- In the absence of individual resource constraints,[2] we develop efficient node prioritization strategies via geometric methods with complexity $O(n \log n)$ for an n-anchor network;
- In the presence of individual resource constraints, we transform the node prioritization problem into that of finding the set generated by the linear combination of vectors with bounded coefficients (LCVBC) and develop an optimal strategy with complexity $O(n^3 \log n)$.

The remaining sections are organized as follows. Section II introduces the system model and formulates node prioritization problems. Section III presents the geometric framework

and demonstrates the sparsity property for the optimal NPV. Sections IV and V respectively provide the optimal solution for the node prioritization problem in the absence and presence of individual resource constraints. A discussion of several related issues is given in Section VI. Finally, the efficiency and the performance gain of the proposed strategies are presented via simulation in Section VII, and conclusions are drawn in Section VIII.

Notation: $[\cdot]^{\mathrm{T}}$ denotes the transpose; $[\boldsymbol{A}]_{ij}$ denotes the element in the ith row and j^{th} column of matrix $\boldsymbol{A}$; $\mathrm{tr}\{\boldsymbol{A}\}$ denotes the trace of a square matrix $\boldsymbol{A}$; $\mathrm{rank}\{\cdot\}$ denotes the rank; $\mathbb{S}_+^n$ denotes the set of $n \times n$ positive-semidefinite matrices; $\|\boldsymbol{x}\|$ denotes the Euclidean norm of vector $\boldsymbol{x}$; $\|\boldsymbol{x}\|_0$ denotes the number of nonzero elements of vector $\boldsymbol{x}$; for vectors $\boldsymbol{x}$ and $\boldsymbol{y}$, the relations $\boldsymbol{x} \succeq \boldsymbol{y}$ and $\boldsymbol{x} \succ \boldsymbol{y}$ denote that all elements of $\boldsymbol{x} - \boldsymbol{y}$ are nonnegative and positive, respectively; matrices $\boldsymbol{A} \succeq \boldsymbol{B}$ denotes that $\boldsymbol{A} - \boldsymbol{B}$ is positive semidefinite; for a set of points $\mathcal{A}$, $\mathbb{H}_{\mathrm{c}}\{\mathcal{A}\}$ denotes the convex hull of $\mathcal{A}$; $\boldsymbol{I}_n$ denotes an $n \times n$ identity matrix, $\boldsymbol{0}_{m,n}$ denotes an $m \times n$ matrix with all 0's, and $\boldsymbol{1}_n$ and $\boldsymbol{0}_n$ denote n-dimensional vectors with all 1's and 0's, respectively, where the subscript will be omitted if clear from the context; $\boldsymbol{e}_k$ is a unit vector with the kth element being 1 and all other elements being 0's; and matrix $\boldsymbol{J}_{\mathrm{r}}(\phi) := [\cos\phi \ \sin\phi]^{\mathrm{T}} [\cos\phi \ \sin\phi]$.

II. PRELIMINARIES

This section introduces the system model, presents the performance metric, and formulates the node prioritization problem for network localization.

A. Problem Formulation

Consider a wireless localization network with n anchors and multiple agents. Anchors are nodes with known positions, whereas agents are nodes with unknown positions. Each agent aims to determine its position based on point-to-point range measurements made with respect to the anchors. Let $\mathcal{N}_{\mathrm{b}} = \{1, 2, \ldots, n\}$ denote the set of anchors and $\boldsymbol{p}_k \in \mathbb{R}^2$ denote the position of anchor $k \in \mathcal{N}_{\mathrm{b}}$. Since the node prioritization problem for each agent has an identical structure, we focus on one agent located at $\boldsymbol{p}_0 \in \mathbb{R}^2$ in the network without loss of generality.

Let $\boldsymbol{J}_{\mathrm{e}}(\boldsymbol{p}_0; \boldsymbol{x})$ denote the FIM for $\boldsymbol{p}_0$, and it is derived in [10] and given as[3]

$$\boldsymbol{J}_{\mathrm{e}}(\boldsymbol{p}_0; \boldsymbol{x}) = \boldsymbol{J}_0 + \sum_{k \in \mathcal{N}_{\mathrm{b}}} \xi_k \, x_k \, \boldsymbol{J}_{\mathrm{r}}(\phi_k) \qquad (1)$$

where $\boldsymbol{J}_0$ is the FIM for the prior positional knowledge, x_k is the amount of resources allocated to anchor k, ξ_k is the equivalent ranging coefficient (ERC) depending on the received waveforms, ϕ_k is the angle from $\boldsymbol{p}_k$ to $\boldsymbol{p}_0$, and $\boldsymbol{x}$ is the NPV, denoted by

$$\boldsymbol{x} := \begin{bmatrix} x_1 \ x_2 \ \ldots \ x_n \end{bmatrix}^{\mathrm{T}}.$$

---

[2] Individual resource constraints refer to the allowable resource consumption for *each* anchor.

[3] If there is no prior positional knowledge, then $\boldsymbol{J}_0 = \boldsymbol{0}_{2,2}$; otherwise, (1) provides an approximation of the FIM in the far field scenario. The exact form of the FIM is discussed in Section VI and we will show such approximation does not change the structure of the problem.

Equation (1) can accommodate various node prioritization problems based on different types of resources manifested in the NPV x, and ERCs ξ_k take corresponding values depending on the type of the resource. The formulation for node prioritization problems based on power and bandwidth resources is given in Appendix I.

The mean squared error of any unbiased estimator $\hat{p}_0$ for position p_0 can be lower bounded by the squared position error bound (SPEB) defined as

$$\mathcal{P}(x) = \text{tr}\{J_{\text{e}}^{-1}(p_0; x)\}. \tag{2}$$

The SPEB is obtained based on the information inequality and is asymptotically achievable by the maximum likelihood estimators in a high signal-to-noise ratio regime (over $10 \sim 15\,\text{dB}$) [36]–[38]. Hence, we adopt the SPEB as the performance metric for network localization. The node prioritization problem is then formulated as follows

$$\mathcal{P} : \underset{x \in \mathbb{R}^n}{\text{minimize}} \quad \mathcal{P}(x)$$

$$\text{subject to} \quad \mathbf{1}^{\text{T}} x \leq 1 \tag{3}$$

$$x \succeq \mathbf{0} \tag{4}$$

$$x \preceq x^{\text{max}} \tag{5}$$

where (3) is the normalized total resource constraint, (4) is the nonnegative constraint for the amount of resources, and (5) is the individual resource constraint.

Remark 1: Parameters such as angles and ERCs are required to solve the node prioritization problems. In applications such as navigation and tracking, these parameters can be estimated from previous time steps. For example, at each step agents estimate those parameters based on the range measurements from anchors, and then use these parameter estimates to determine the node prioritization strategy for the next time step.[4]

Remark 2: The methods developed in this paper are also applicable to the problems using other performance metrics (e.g., the smaller eigenvalue or the determinant of the FIM) and to some other formulations of the node prioritization problems (e.g., minimizing the total resource consumption subject to a given localization performance requirement).

In the following sections, the problem without the individual resource constraint (5) is first investigated, and the generalization to the problem with the individual resource constraint is given in Section V. For the ease of exposition, the problem $\mathcal{P}$ without the individual constraint (5) is denoted as $\mathcal{P}_0$.

B. Properties of SPEB

This subsection introduces two important properties of the SPEB.

Proposition 1 (Convexity [32]): The SPEB $\mathcal{P}(x)$ is a convex function of $x \succeq \mathbf{0}$.

Remark 3: This proposition implies that the node prioritization problem $\mathcal{P}$ is a convex program and can be solved by standard convex optimization engines. In addition, the

---

[4] Note that the estimated parameters may be subject to uncertainties. In Section VI, we will present a robust formulation to deal with these uncertainties.

problem $\mathcal{P}$ can be transformed into SDP [32] and SOCP [29], which have more efficient solvers than general convex programs.

Proposition 2 (Monotonicity [39]): For two NPVs x and y, if $x \succeq y$, then $\mathcal{P}(x) \leq \mathcal{P}(y)$.

Remark 4: Proposition 2 implies that (3) can be replaced with the equality $\mathbf{1}^{\text{T}} x = 1$. Moreover, if $\mathbf{1}^{\text{T}} x^{\text{max}} \leq 1$, the optimal solution can be trivially obtained as $x = x^{\text{max}}$ due to the monotonicity. Hence, we only consider the case where $\mathbf{1}^{\text{T}} x^{\text{max}} > 1$.

III. GEOMETRIC FRAMEWORK AND SPARSITY PROPERTY

This section formulates the geometric framework for the node prioritization problem $\mathcal{P}_0$ and shows the sparsity property of the optimal NPV.

A. Reduced Dimension of NPV

The following proposition gives a fractional expression of the SPEB defined in (2).

Proposition 3: The SPEB $\mathcal{P}(x)$ can be written as follows

$$\mathcal{P}(x) = \frac{4\,y_3}{y_3^2 - y_1^2 - y_2^2} \tag{6}$$

where

$$y_1 = c^{\text{T}} R\, x - [J_0]_{22} + [J_0]_{11}$$
$$y_2 = s^{\text{T}} R\, x + 2[J_0]_{12}$$
$$y_3 = \mathbf{1}^{\text{T}} R\, x + \text{tr}\{J_0\}$$

in which $R = \text{diag}\{\xi_1, \xi_2, \dots, \xi_n\}$, and

$$c = [\cos 2\phi_1 \quad \cos 2\phi_2 \quad \dots \quad \cos 2\phi_n]^{\text{T}}$$
$$s = [\sin 2\phi_1 \quad \sin 2\phi_2 \quad \dots \quad \sin 2\phi_n]^{\text{T}}.$$

Proof: Note that the FIM can be written as

$$J_{\text{e}}(p_0; x) = J_0 + \sum_{k \in \mathcal{N}_{\text{b}}} \xi_k x_k J_{\text{r}}(\phi_k)$$

$$= J_0 + \sum_{k \in \mathcal{N}_{\text{b}}} \xi_k x_k \begin{bmatrix} \cos^2 \phi_k & \sin \phi_k \cos \phi_k \\ \sin \phi_k \cos \phi_k & \sin^2 \phi_k \end{bmatrix}$$

$$= J_0 + \sum_{k \in \mathcal{N}_{\text{b}}} \frac{\xi_k x_k}{2} \begin{bmatrix} 1 + \cos 2\phi_k & \sin 2\phi_k \\ \sin 2\phi_k & 1 - \cos 2\phi_k \end{bmatrix}$$

$$= \begin{bmatrix} (y_3 + y_1)/2 & y_2/2 \\ y_2/2 & (y_3 - y_1)/2 \end{bmatrix}.$$

Consequently, the SPEB $\mathcal{P}(x)$ can be written as

$$\mathcal{P}(x) = \text{tr}\left\{ \begin{bmatrix} (y_3 + y_1)/2 & y_2/2 \\ y_2/2 & (y_3 - y_1)/2 \end{bmatrix}^{-1} \right\}$$

which is equivalent to (6) after some algebra. $\quad\square$

Remark 5: The following observation, essential for the design of efficient node prioritization strategies, can be made from Proposition 3: the SPEB can be written as a function of only three variables, each of which is an affine function of (possibly high-dimensional) an NPV.

Fig. 2.   Convex polyhedron $\mathcal{Y}$ and one side of two-sheeted hyperboloid prescribed by (8).
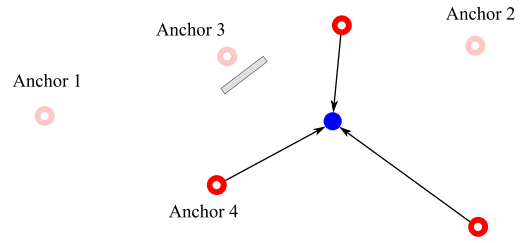

Fig. 3.   Illustration of the sparsity: resources can be optimally allocated to only three active anchors. Most anchors will not be used due to unfavorable channel qualities or poor network geometry.

Equation (6) suggests an affine transformation that maps an NPV $\boldsymbol{x}$ to a point in three-dimensional space

$$\boldsymbol{y} = \boldsymbol{A}\,\boldsymbol{x} + \boldsymbol{b}$$

where $\boldsymbol{A} = [\,\boldsymbol{c}\ \ \boldsymbol{s}\ \ \boldsymbol{1}\,]^{\mathrm{T}}\boldsymbol{R}$ and

$$\boldsymbol{b} = \big[\,-[\boldsymbol{J}_0]_{22} + [\boldsymbol{J}_0]_{11}\quad -2\cdot[\boldsymbol{J}_0]_{12}\quad \mathrm{tr}\{\boldsymbol{J}_0\}\,\big]^{\mathrm{T}}.$$

Proposition 3 implies that

$$\boldsymbol{Q}(\boldsymbol{y}) := \frac{4\,y_3}{y_3^2 - y_1^2 - y_2^2} = \mathcal{P}(\boldsymbol{x}). \tag{7}$$

This leads to the geometric representation of the SPEB in the next proposition.

Proposition 4: Given an NPV $\boldsymbol{x}$, the point $\boldsymbol{y} = \boldsymbol{A}\,\boldsymbol{x} + \boldsymbol{b}$ lies on a hyperboloid, given by

$$\big(y_3 - 2\lambda^{-1}\big)^2 - y_1^2 - y_2^2 - 4\lambda^{-2} = 0 \tag{8}$$

where $\lambda = \mathcal{P}(\boldsymbol{x})$.

Proof: For $\lambda = \mathcal{P}(\boldsymbol{x})$, we have $\boldsymbol{Q}(\boldsymbol{y}) = \lambda$. Note that for a given $\lambda > 0$ and $\boldsymbol{y} \in \mathbb{R}^3$, $\boldsymbol{Q}(\boldsymbol{y}) = \lambda$ depicts a quadratic curve, identical to curve (8) except at $\boldsymbol{y} = \boldsymbol{0}$. $\qquad\square$

Denote the feasible NPV set and its image set, respectively, by

$$\mathcal{X} = \big\{\boldsymbol{x} \in \mathbb{R}^n : \boldsymbol{1}^{\mathrm{T}}\boldsymbol{x} = 1, \boldsymbol{0} \preceq \boldsymbol{x}\big\}$$

and

$$\mathcal{Y} = \big\{\boldsymbol{y} \in \mathbb{R}^3 : \boldsymbol{y} = \boldsymbol{A}\,\boldsymbol{x} + \boldsymbol{b}, \boldsymbol{x} \in \mathcal{X}\big\}.$$

Note that each element $\boldsymbol{x} \in \mathcal{X}$ can be written as a convex combination of elements in

$$\mathcal{E} := \{\boldsymbol{e}_1, \boldsymbol{e}_2, \ldots, \boldsymbol{e}_n\}.$$

The next proposition provides a geometric property of $\mathcal{Y}$.

Proposition 5: The image set $\mathcal{Y}$ is a convex polyhedron, given by $\mathbb{H}_{\mathrm{c}}\{\boldsymbol{A}\,\boldsymbol{e} + \boldsymbol{b} : \boldsymbol{e} \in \mathcal{E}\}$.

Proof: For any $\boldsymbol{x} \in \mathcal{X}$, $\boldsymbol{y} = \sum_{k=1}^{n} x_k(\boldsymbol{A}\,\boldsymbol{e}_k + \boldsymbol{b})$ with $\sum_{k=1}^{n} x_k = 1$. Thus, $\boldsymbol{y}$ is a convex combination of $\boldsymbol{A}\,\boldsymbol{e}_k + \boldsymbol{b}$, $k = 1, 2, \ldots, n$. Therefore, $\mathcal{Y}$ is the convex hull of points $\mathbb{H}_{\mathrm{c}}\{\boldsymbol{A}\,\boldsymbol{e} + \boldsymbol{b} : \boldsymbol{e} \in \mathcal{E}\}$. $\qquad\square$

This proposition implies that for $\boldsymbol{x} \in \mathcal{X}$ with the corresponding SPEB $\lambda = \mathcal{P}(\boldsymbol{x})$, $\boldsymbol{A}\,\boldsymbol{x} + \boldsymbol{b}$ is in the intersection of $\mathcal{Y}$ and curve (8), as illustrated in Fig. 2.

B. Geometric Properties of the Optimal NPV

Based on the above geometric observations, some properties of the optimal NPV are obtained in this section.

Proposition 6: If $\boldsymbol{x}^*$ is an optimal solution for $\mathscr{P}_0$, then $\boldsymbol{y}^* = \boldsymbol{A}\,\boldsymbol{x}^* + \boldsymbol{b}$ lies on the surface of the convex polyhedron $\mathcal{Y}$.

Proof: Suppose $\boldsymbol{y}^*$ is an interior point of $\mathcal{Y}$, then by the definition of interior points, there exists $\epsilon > 0$ such that

$$\{\boldsymbol{y} : \|\boldsymbol{y} - \boldsymbol{y}^*\| \le \epsilon\} \subseteq \mathcal{Y}.$$

Let $\delta = \epsilon/(2\cdot\|\boldsymbol{A}\,\boldsymbol{1}\|)$ and $\boldsymbol{x}_\delta = \boldsymbol{x}^* + \delta\boldsymbol{1}$.[5] Clearly,

$$|\boldsymbol{A}\,\boldsymbol{x}_\delta + \boldsymbol{b} - \boldsymbol{y}^*| \le \epsilon.$$

Therefore, $\boldsymbol{y}_\delta = \boldsymbol{A}\,\boldsymbol{x}_\delta + \boldsymbol{b} \in \mathcal{Y}$, and by Proposition 5, there exists $\tilde{\boldsymbol{x}} \in \mathcal{X}$ such that $\boldsymbol{y}_\delta = \sum_{k\in\mathcal{N}_{\mathrm{b}}} \tilde{x}_k(\boldsymbol{A}\,\boldsymbol{e}_k + \boldsymbol{b}) = \boldsymbol{A}\tilde{\boldsymbol{x}} + \boldsymbol{b}$. Equation (7) gives

$$\begin{aligned}\mathcal{P}(\boldsymbol{x}_\delta) &= \boldsymbol{Q}(\boldsymbol{A}\,\boldsymbol{x}_\delta + \boldsymbol{b})\\ &= \boldsymbol{Q}(\boldsymbol{A}\,\tilde{\boldsymbol{x}} + \boldsymbol{b}) = \mathcal{P}(\tilde{\boldsymbol{x}})\end{aligned}$$

where the second equality is because $\boldsymbol{A}\,\boldsymbol{x}_\delta + \boldsymbol{b} = \boldsymbol{y}_\delta = \boldsymbol{A}\tilde{\boldsymbol{x}} + \boldsymbol{b}$. Since $\boldsymbol{x}^*$ is the optimal NPV, $\mathcal{P}(\boldsymbol{x}^*) \le \mathcal{P}(\tilde{\boldsymbol{x}})$. Thus we have $\mathcal{P}(\boldsymbol{x}^*) \le \mathcal{P}(\boldsymbol{x}_\delta)$. This is a contradiction since $\boldsymbol{x}_\delta = \boldsymbol{x}^* + \delta\boldsymbol{1}$, implying that $\mathcal{P}(\boldsymbol{x}_\delta) < \mathcal{P}(\boldsymbol{x}^*)$. $\qquad\square$

With Proposition 6, we determine the sparsity property of the optimal NPV.

Theorem 1: In two-dimensional networks, there exists an optimal NPV $\boldsymbol{x}$ for $\mathscr{P}_0$ such that $\|\boldsymbol{x}\|_0 \le 3$.

Proof: Suppose $\boldsymbol{x}^*$ is an optimal solution for $\mathscr{P}_0$. By Proposition 6, $\boldsymbol{y}^* = \boldsymbol{A}\,\boldsymbol{x}^* + \boldsymbol{b}$ lies on the surface of $\mathcal{Y}$, and hence inside a triangle with three vertices, denoted by $\boldsymbol{A}\,\boldsymbol{e}_i + \boldsymbol{b}$, $\boldsymbol{A}\,\boldsymbol{e}_j + \boldsymbol{b}$, and $\boldsymbol{A}\,\boldsymbol{e}_k + \boldsymbol{b}$. Thus $\boldsymbol{y}^*$ can be written as a convex combination: $\boldsymbol{y}^* = x_i(\boldsymbol{A}\,\boldsymbol{e}_i + \boldsymbol{b}) + x_j(\boldsymbol{A}\,\boldsymbol{e}_j + \boldsymbol{b}) + x_k(\boldsymbol{A}\,\boldsymbol{e}_k + \boldsymbol{b})$ for nonnegative x_i, x_j and x_k such that $x_i + x_j + x_k = 1$. Let $\boldsymbol{x} = x_i\boldsymbol{e}_i + x_j\boldsymbol{e}_j + x_k\boldsymbol{e}_k$, then $\boldsymbol{A}\,\boldsymbol{x} = \boldsymbol{A}\,\boldsymbol{x}^*$ and

$$\begin{aligned}\mathcal{P}(\boldsymbol{x}) &= \boldsymbol{Q}(\boldsymbol{A}\,\boldsymbol{x} + \boldsymbol{b})\\ &= \boldsymbol{Q}(\boldsymbol{A}\,\boldsymbol{x}^* + \boldsymbol{b}) = \mathcal{P}(\boldsymbol{x}^*).\end{aligned}$$

Hence, $\boldsymbol{x}$ is also an optimal solution for $\mathscr{P}_0$ with $\|\boldsymbol{x}\|_0 \le 3$. $\qquad\square$

Remark 6: Theorem 1 implies that the total transmission resources can be allocated to only three anchors without loss of optimality in two-dimensional networks. We intuit that most anchors will not be used due to unfavorable channel qualities or poor network geometry. For example in Fig. 3,

---

[5]One can verify that $\boldsymbol{A}\,\boldsymbol{1} \ne \boldsymbol{0}$ and hence δ is well defined.

Anchor 1 is not active since it is farther away from the agent compared to other anchors. Therefore, the same amount of resources allocated to other anchors contribute more in reducing the SPEB. Anchor 2 forms almost a straight line with the agent and Anchor 4, and thus, Anchor 2 and Anchor 4 provide information along the similar direction. However, since Anchor 4 is closer than Anchor 2 to the agent, the same amount of resources in Anchor 4 provides more information along the aforementioned direction, and thus Anchor 2 is not used.

C. More Results on the Sparsity Property

Theorem 1 reveals the sparsity property of the optimal NPV for two-dimensional networks. In fact, this sparsity property is also retained for networks in high dimension. Note that in the high-dimensional case, the FIM is

$$\boldsymbol{J}_{\mathrm{e}}(\boldsymbol{p}_0; \boldsymbol{x}) = \boldsymbol{J}_0 + \sum_{k \in \mathcal{N}_{\mathrm{b}}} \xi_k \, x_k \, \boldsymbol{u}_k \, \boldsymbol{u}_k^{\mathrm{T}} \qquad (9)$$

where $\boldsymbol{u}_k = (\boldsymbol{p}_k - \boldsymbol{p}_0)/\|\boldsymbol{p}_k - \boldsymbol{p}_0\|$ and the corresponding SPEB is $\mathcal{P}(\boldsymbol{x}) = \mathrm{tr}\left\{\boldsymbol{J}_{\mathrm{e}}^{-1}(\boldsymbol{p}_0; \boldsymbol{x})\right\}$.

Theorem 2: There exists an optimal NPV $\boldsymbol{x}$ for $\mathscr{P}_0$ such that $\|\boldsymbol{x}\|_0 \leq D$ in d-dimensional networks, where $D = \binom{d+1}{2}$.

Proof: For any symmetric $d \times d$ matrix $\boldsymbol{M}$, we denote a one-to-one function $\boldsymbol{f} \colon \mathbb{R}^{d \times d} \to \mathbb{R}^D$, such that $\boldsymbol{f}(\boldsymbol{M})$ is a $D \times 1$ vector obtained by rearranging D elements in the upper triangular part of $\boldsymbol{M}$.

Note that $\boldsymbol{J}_{\mathrm{e}}(\boldsymbol{p}_0; \boldsymbol{x})$ is a symmetric $d \times d$ matrix and each element of $\boldsymbol{J}_{\mathrm{e}}(\boldsymbol{p}_0; \boldsymbol{x})$ is an affine function of $\boldsymbol{x}$. Hence, there exists a matrix $\boldsymbol{B}$ and vector $\boldsymbol{c}$ such that

$$\boldsymbol{B}\,\boldsymbol{x} + \boldsymbol{c} = \boldsymbol{f}\big(\boldsymbol{J}_{\mathrm{e}}(\boldsymbol{p}_0; \boldsymbol{x})\big).$$

Consequently, we can rewrite the SPEB as

$$\mathcal{P}(\boldsymbol{x}) = \mathrm{tr}\left\{\left(\boldsymbol{f}^{(-1)}(\boldsymbol{B}\,\boldsymbol{x} + \boldsymbol{c})\right)^{-1}\right\}$$
$$=: g(\boldsymbol{B}\,\boldsymbol{x} + \boldsymbol{c})$$

where $\boldsymbol{f}^{(-1)}(\cdot)$ is the inverse function of $\boldsymbol{f}(\cdot)$.

Let $\mathcal{Y}^{\mathrm{D}} = \{\boldsymbol{y} \in \mathbb{R}^D : \boldsymbol{y} = \boldsymbol{B}\,\boldsymbol{x} + \boldsymbol{c}, \boldsymbol{x} \in \mathcal{X}\}$. One can verify that $\mathcal{Y}^{\mathrm{D}}$ is a convex polytope, given by

$$\mathbb{H}_{\mathrm{c}}\{\boldsymbol{B}\,\boldsymbol{e}_1 + \boldsymbol{c}, \, \boldsymbol{B}\,\boldsymbol{e}_2 + \boldsymbol{c}, \, \ldots, \boldsymbol{B}\,\boldsymbol{e}_n + \boldsymbol{c}\}.$$

Similarly to Proposition 6, if $\boldsymbol{x}^*$ is an optimal solution for $\mathscr{P}_0$, then $\boldsymbol{y}^* = \boldsymbol{B}\,\boldsymbol{x}^* + \boldsymbol{c}$ lies on the boundary of the convex polytope $\mathcal{Y}^{\mathrm{D}}$, and hence inside a $(D-1)$-simplex with D vertices, denoted by $\boldsymbol{B}\,\boldsymbol{e}_{k_1} + \boldsymbol{c}, \boldsymbol{B}\,\boldsymbol{e}_{k_2} + \boldsymbol{c}, \ldots, \boldsymbol{B}\,\boldsymbol{e}_{k_D} + \boldsymbol{c}$. Thus, $\boldsymbol{y}^*$ can be written as a convex combination:

$$\boldsymbol{y}^* = \sum_{j=1}^{D} x_j (\boldsymbol{B}\,\boldsymbol{e}_{k_j} + \boldsymbol{c})$$

for nonnegative $x_j (1 \leq j \leq D)$ such that $\sum_{j=1}^{D} x_j = 1$. Let $\boldsymbol{x} = \sum_{j=1}^{D} x_j \boldsymbol{e}_{k_j}$. Then $\boldsymbol{B}\,\boldsymbol{x} = \boldsymbol{B}\,\boldsymbol{x}^*$ and

$$\mathcal{P}(\boldsymbol{x}) = g(\boldsymbol{B}\,\boldsymbol{x} + \boldsymbol{c})$$
$$= g(\boldsymbol{B}\,\boldsymbol{x}^* + \boldsymbol{c}) = \mathcal{P}(\boldsymbol{x}^*).$$

Hence, $\boldsymbol{x}$ is also an optimal solution for $\mathscr{P}_0$ with $\|\boldsymbol{x}\|_0 \leq D$. $\qquad \square$

Theorem 2 is a generalization of Theorem 1. For two-dimensional case, a stronger result is provided as follows.

Proposition 7: For two-dimensional node prioritization problem $\mathscr{P}_0$, there exists an optimal solution $\boldsymbol{x}^*$ such that $\|\boldsymbol{x}^*\|_0 \leq \mathrm{rank}\{\boldsymbol{\Lambda}\}$, where

$$\boldsymbol{\Lambda} = \boldsymbol{1}\,\boldsymbol{1}^{\mathrm{T}} - \boldsymbol{c}\,\boldsymbol{c}^{\mathrm{T}} - \boldsymbol{s}\,\boldsymbol{s}^{\mathrm{T}}.$$

Note that $\mathrm{rank}\{\boldsymbol{\Lambda}\} \leq 3$ since $\boldsymbol{\Lambda} = \boldsymbol{1}\,\boldsymbol{1}^{\mathrm{T}} - \boldsymbol{c}\,\boldsymbol{c}^{\mathrm{T}} - \boldsymbol{s}\,\boldsymbol{s}^{\mathrm{T}}$. It can be shown that this inequality is strict for certain topologies. Consequently, Proposition 7 provides a tighter upper bound than Theorem 1. An alternative proof of Theorem 2 and the proof of Proposition 7 via algebraic methods are shown in Appendix II and Appendix III, respectively.

IV. GEOMETRIC METHODS FOR DETERMINING THE OPTIMAL NPV

This section presents the geometric methods for determining the optimal NPV of $\mathscr{P}_0$. The sparsity property implies that the quest for the optimal NPV can be restricted to the small networks with three anchors, referred to as *simple networks*. The simple network that the optimal NPV corresponds to is referred to as the *optimal simple network*. We first design the optimal node prioritization strategies for simple networks in Section IV-A, and then propose a geometric method to efficiently find the optimal simple network in Sections IV-B and IV-C. The discussion on computational complexity is presented in Section IV-D.

A. Optimal NPVs in Simple Networks

Given three feasible NPVs $\boldsymbol{x}_1$, $\boldsymbol{x}_2$ and $\boldsymbol{x}_3$, consider a set $\mathcal{V}$ consisting of all NPVs that can be written as a convex combination of these three NPVs, i.e.,

$$\mathcal{V} := \left\{\boldsymbol{x} = \sum_{k=1}^{3} \omega_k \, \boldsymbol{x}_k : \sum_{k=1}^{3} \omega_k = 1, \omega_k \geq 0\right\}.$$

The goal is to determine an NPV with the smallest SPEB among this set, i.e.,

$$\mathscr{P}_{\mathrm{S}} : \quad \begin{aligned} &\underset{\boldsymbol{x} \in \mathbb{R}^3}{\text{minimize}} && \mathcal{P}(\boldsymbol{x}) \\ &\text{subject to} && \boldsymbol{x} \in \mathcal{V}. \end{aligned}$$

Note that the solution of $\mathscr{P}_0$ in a simple network can be obtained from that of $\mathscr{P}_{\mathrm{S}}$ by setting $\boldsymbol{x}_k = \boldsymbol{e}_k$, $k \in \{1, 2, 3\}$.

The geometric interpretation of SPEB in Proposition 4 is used to solve the problem $\mathscr{P}_{\mathrm{S}}$. Let $\mathcal{U}$ denote the image set of NPVs from $\mathcal{V}$ under transformation $\boldsymbol{A}\,\boldsymbol{x} + \boldsymbol{b}$, i.e.,

$$\mathcal{U} := \{\boldsymbol{A}\,\boldsymbol{x} + \boldsymbol{b} : \boldsymbol{x} \in \mathcal{V}\}.$$

Clearly, $\mathcal{U}$ consists of all vectors that can be written as a convex combination of $\boldsymbol{u}_k = \boldsymbol{A}\,\boldsymbol{x}_k + \boldsymbol{b}$, $k \in \{1, 2, 3\}$. Moreover, for $\lambda > 0$, let

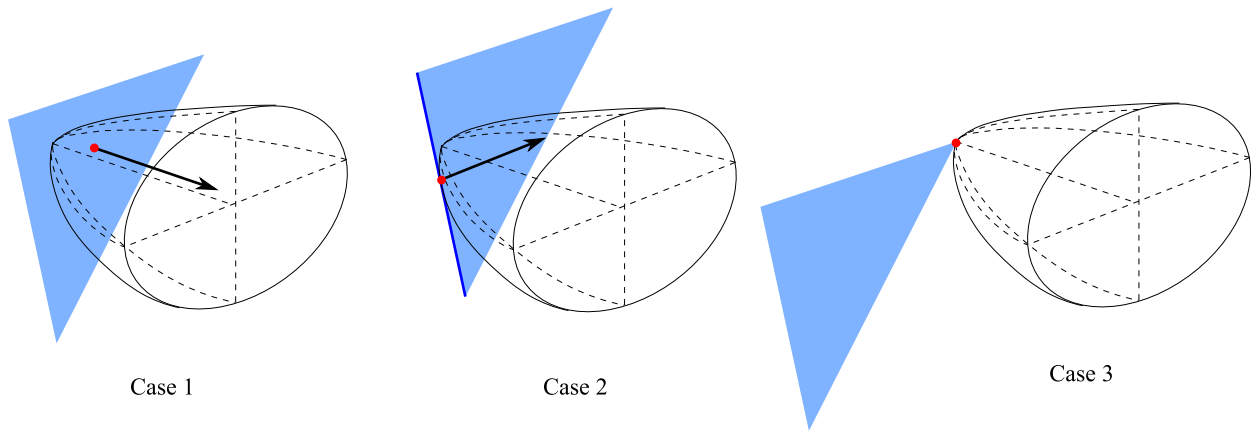$$\mathcal{H}(\lambda) = \left\{\boldsymbol{y} \in \mathbb{R}^3 : y_1, y_2, \text{and } y_3 \text{ satisfy (8)}\right\}.$$

Fig. 4.   Illustration of different cases for solving $\mathscr{P}_{\mathrm{G}}$: in Case 1, $\mathcal{U}$ is a triangle and $\boldsymbol{y}^\circ$ is an interior point of $\mathcal{U}$; in Case 2, $\mathcal{U}$ is a triangle and $\boldsymbol{y}^\circ$ is on the edge of $\mathcal{U}$, but not a vertex of $\mathcal{U}$; and in Case 3, $\mathcal{U}$ is a triangle and $\boldsymbol{y}^\circ$ is a vertex of $\mathcal{U}$. Case 4 is not illustrated since it is similar to Case 2 and 3.

The next proposition shows that the solution of the problem $\mathscr{P}_{\mathrm{S}}$ can be obtained from that of the following problem

$$\mathscr{P}_{\mathrm{G}} : \quad \underset{\lambda_1 > 0}{\text{minimize}} \quad \lambda_1$$
$$\text{subject to} \quad \mathcal{U} \cap \mathcal{H}(\lambda_1) \neq \varnothing.$$

Proposition 8: For any $\boldsymbol{x}^\circ \in \mathcal{V}$, if $\boldsymbol{A}\boldsymbol{x}^\circ + \boldsymbol{b} \in \mathcal{H}(\lambda_1^\circ)$, where λ_1° is the optimal solution for $\mathscr{P}_{\mathrm{G}}$, then $\boldsymbol{x}^\circ$ is an optimal solution for $\mathscr{P}_{\mathrm{S}}$.

Proof: Suppose $\boldsymbol{x}^*$ is an optimal solution for $\mathscr{P}_{\mathrm{S}}$. By Proposition 4, $\boldsymbol{y}^* = \boldsymbol{A}\boldsymbol{x}^* + \boldsymbol{b} \in \mathcal{H}(\lambda_1^*)$, where $\lambda_1^* = \mathcal{P}(\boldsymbol{x}^*)$. Clearly, $\boldsymbol{y}^* \in \mathcal{U}$. Hence, $\mathcal{U} \cap \mathcal{H}(\lambda_1^*) \neq \varnothing$, implying that λ_1^* is a feasible value of $\mathscr{P}_{\mathrm{G}}$. Therefore, $\lambda_1^\circ \leq \lambda_1^*$ since λ_1° is the optimal value for $\mathscr{P}_{\mathrm{G}}$.

It can be shown that $\boldsymbol{A}\boldsymbol{x}^\circ + \boldsymbol{b} \in \mathcal{H}(\lambda_1^\circ)$ implies that $\mathcal{P}(\boldsymbol{x}^\circ) = \lambda_1^\circ$. Since $\boldsymbol{x}^\circ \in \mathcal{V}$, $\boldsymbol{x}^\circ$ is a feasible solution of $\mathscr{P}_{\mathrm{S}}$. Therefore, $\mathcal{P}(\boldsymbol{x}^*) \leq \mathcal{P}(\boldsymbol{x}^\circ)$ since $\boldsymbol{x}^*$ is the optimal solution for $\mathscr{P}_{\mathrm{S}}$. Equivalently, $\lambda_1^* \leq \lambda_1^\circ$. Consequently, $\mathcal{P}(\boldsymbol{x}^*) = \mathcal{P}(\boldsymbol{x}^\circ)$ and hence $\boldsymbol{x}^\circ$ is also an optimal solution for $\mathscr{P}_{\mathrm{S}}$. $\square$

Note that with the optimal solution of $\mathscr{P}_{\mathrm{G}}$, λ_1°, and a point $\boldsymbol{y}^\circ \in \mathcal{U} \cap \mathcal{H}(\lambda_1^\circ)$, one can obtain nonnegative ω_1°, ω_2° and ω_3° such that $\boldsymbol{y}^\circ = \sum_{k=1}^3 \omega_k^\circ \boldsymbol{u}_k$ and $\sum_{k=1}^3 \omega_k^\circ = 1$. Consider a vector $\boldsymbol{x}^\circ = \sum_{k=1}^3 \omega_k^\circ \boldsymbol{x}_k$, then one can verify that $\boldsymbol{x}^\circ \in \mathcal{V}$ and $\boldsymbol{A}\boldsymbol{x}^\circ + \boldsymbol{b} \in \mathcal{H}(\lambda_1^\circ)$, and hence $\boldsymbol{x}^\circ$ is an optimal solution for $\mathscr{P}_{\mathrm{S}}$ by Proposition 8.

Next we determine an optimal solution λ_1° of $\mathscr{P}_{\mathrm{G}}$ and $\boldsymbol{y}^\circ \in \mathcal{U} \cap \mathcal{H}(\lambda_1^\circ)$ using the geometric method. The approach of finding an optimal solution can be divided into four cases, depending on the shape of $\mathcal{U}$ and the position of $\boldsymbol{y}^\circ$ relative to $\mathcal{U}$. The illustration of different cases are shown in Fig. 4.

- Case 1: $\mathcal{U}$ is a triangle and $\boldsymbol{y}^\circ$ is an interior point of $\mathcal{U}$.
  Any point $[\, x_1 \ x_2 \ x_3 \,]^{\mathrm{T}}$ on the plane containing $\mathcal{U}$ satisfies

$$c_3 x_1 + c_2 x_2 + c_1 x_3 + c_0 = 0$$

  where the coefficients c_k depend on $\mathcal{U}$ and assume that $c_0 > 0$. Since $\boldsymbol{y}^\circ$ is an interior point of $\mathcal{U}$, the triangle $\mathcal{U}$ is tangent to $\mathcal{H}(\lambda_1^\circ)$ at $\boldsymbol{y}^\circ$. Thus, normal vectors of $\mathcal{U}$ and $\mathcal{H}(\lambda_1^\circ)$ are aligned at $\boldsymbol{y}^\circ$, implying that there exists t such that

$$t\,\boldsymbol{c} = \left[\, -y_1^\circ \quad -y_2^\circ \quad (y_3^\circ - 2/\lambda_1^\circ) \,\right]^{\mathrm{T}} \quad (10)$$

where $\boldsymbol{c} = [\, c_3 \ c_2 \ c_1 \,]^{\mathrm{T}}$. Moreover, since $\boldsymbol{y}^\circ$ lies in both $\mathcal{U}$ and $\mathcal{H}(\lambda_1^\circ)$,

$$c_3 y_1^\circ + c_2 y_2^\circ + c_1 y_3^\circ + c_0 = 0$$
$$\left(y_3^\circ - 2/\lambda_1^\circ\right)^2 - y_1^{\circ 2} - y_2^{\circ 2} - 4(\lambda_1^\circ)^{-2} = 0. \quad (11)$$

Solving the equations above gives

$$\lambda_1^\circ = \frac{2\sqrt{c_1^2 - c_2^2 - c_3^2} - 2\,c_1}{c_0} \quad (12)$$

$$t = \frac{c_0 + 2c_1/\lambda_1^\circ}{c_3^2 + c_2^2 - c_1^2} \quad (13)$$

and $\boldsymbol{y}^\circ$ can be obtained by substituting (12) and (13) into (10).

- Case 2: $\mathcal{U}$ is a triangle and $\boldsymbol{y}^\circ$ is on the edge of $\mathcal{U}$, but not a vertex of $\mathcal{U}$.
  Without loss of generality, suppose the edge containing $\boldsymbol{y}^\circ$ connects $\boldsymbol{u}_1$ and $\boldsymbol{u}_2$, and therefore $\boldsymbol{y}^\circ$ can be written as

$$\boldsymbol{y}^\circ = \boldsymbol{u}_1 + t\,(\boldsymbol{u}_2 - \boldsymbol{u}_1) \quad (14)$$

  for some $t \in (0, 1)$. Let $[\, a_1 \ a_2 \ a_3 \,]^{\mathrm{T}} = \boldsymbol{u}_1$ and $[\, b_1 \ b_2 \ b_3 \,]^{\mathrm{T}} = \boldsymbol{u}_2 - \boldsymbol{u}_1$. Since $\boldsymbol{y}^\circ$ is an interior point of the edge, $\boldsymbol{u}_1 - \boldsymbol{u}_2$ is orthogonal to the normal vector of $\mathcal{H}$ at $\boldsymbol{y}^\circ$, i.e.,

$$-y_1^\circ b_1 - y_2^\circ b_2 + (y_3 - 2/\lambda_1^\circ)b_3 = 0. \quad (15)$$

Substituting (14) into (15) and (11) gives

$$A_2\,t^2 + A_1\,t + A_0 = 0 \quad (16)$$

where

$$A_2 = b_3\,(b_3^2 - b_2^2 - b_1^2)$$
$$A_1 = 2\,a_3\,(b_3^2 - b_2^2 - b_1^2)$$
$$A_0 = 2\,a_3\,(a_3 b_3 - a_2 b_2 - a_1 b_1) - b_3\,(a_3^2 - a_2^2 - a_1^2).$$

Then a closed-form solution of t can be obtained. The expression of $\boldsymbol{y}^\circ$ can be obtained accordingly.

- Case 3: $\mathcal{U}$ is a triangle and $\boldsymbol{y}^\circ$ is a vertex of $\mathcal{U}$.

Algorithm 1 Solution to Problem $\mathscr{P}_{\mathrm{G}}$

Input: $\mathcal{U}$
Output: λ_1° and $\boldsymbol{y}^\circ$
1: **if** $\mathcal{U}$ is a triangle **then**
2:      Compute λ_1° from (12) and the corresponding $\boldsymbol{y}^\circ$;
3:      **if** $\boldsymbol{y}^\circ$ is in $\mathcal{U}$ **then**
4:          Output λ_1° and $\boldsymbol{y}^\circ$;
5:      **else**
6:          Compute λ_1° from (14)-(16) and the corresponding $\boldsymbol{y}^\circ$;
7:          **if** $\boldsymbol{y}^\circ$ is in one of $\mathcal{U}$'s edges but not a vertex **then**
8:              Output λ_1° and $\boldsymbol{y}^\circ$;
9:          **else**
10:              Obtain λ_1° and $\boldsymbol{y}^\circ$ according to Case 3;
11:              Output λ_1° and $\boldsymbol{y}^\circ$;
12:          **end if**
13:      **end if**
14: **else**
15:      Obtain λ_1° and $\boldsymbol{y}^\circ$ according to Case 4;
16: **end if**

Algorithm 2 Node Prioritization via Geometric Methods (NPGM)

Input: ξ_k and ϕ_k, $k \in \mathcal{N}_{\mathrm{b}}$
Output: Optimal NPV $\boldsymbol{x}^*$ for $\mathscr{P}_0$
1: Initialization: $\boldsymbol{x}^* \leftarrow \mathbf{1}/n$ and $\mathcal{P}_{\mathrm{tmp}} \leftarrow \mathcal{P}(\mathbf{1}/n)$;
2: Construct $\mathcal{Y} = \mathbb{H}_{\mathrm{c}}\{\boldsymbol{A}\,\boldsymbol{e} + \boldsymbol{b} : \boldsymbol{e} \in \mathcal{E}\}$;
3: Find a triangulation for the faces of $\mathcal{Y}$ and let $\mathcal{K}$ denote the set consisting of all the resulting triangles;
4: **repeat**
5:      Find an element $K_i \in \mathcal{K}$ and let $\boldsymbol{A}\,\boldsymbol{e}_{i_1} + \boldsymbol{b}$, $\boldsymbol{A}\,\boldsymbol{e}_{i_2} + \boldsymbol{b}$ and $\boldsymbol{A}\,\boldsymbol{e}_{i_3} + \boldsymbol{b}$ denote the vertices of K_i;
6:      Find the optimal NPV $\boldsymbol{x}_{\mathrm{tmp}}$ according to Proposition 8 and Algorithm 1 for the simple network $\{i_1, i_2, i_3\}$;
7:      **if** $\mathcal{P}(\boldsymbol{x}_{\mathrm{tmp}}) \leq \mathcal{P}_{\mathrm{tmp}}$ **then**
8:          $\mathcal{P}_{\mathrm{tmp}} \leftarrow \mathcal{P}(\boldsymbol{x}_{\mathrm{tmp}})$;
9:          $\boldsymbol{x}^* \leftarrow \boldsymbol{x}_{\mathrm{tmp}}$;
10:      **end if**
11:      $\mathcal{K} \leftarrow \mathcal{K} \setminus \{K_i\}$;
12: **until** $\mathcal{K} = \varnothing$
13: Output $\boldsymbol{x}^*$.

In this case, $\boldsymbol{y}^\circ$ is the vertex with the smallest λ_1°.
- Case 4: $\mathcal{U}$ degenerates to a segment or a point.
  The solution can be obtained similarly to that in Case 2 or Case 3.

The observations made in the above four cases lead to Algorithm 1 for finding λ_1° and $\boldsymbol{y}^\circ$.

Remark 7: In node prioritization problems, Karush-Kuhn-Tucker (KKT) conditions often play an important role in determining the optimal solutions [40]. In particular, Appendix IV provides an alternative way of solving $\mathscr{P}_0$ in simple networks via checking KKT conditions.

B. Optimal Simple Networks

We next show how to efficiently find the optimal simple network. Let $\boldsymbol{x}^*$ be an optimal NPV for $\mathscr{P}_0$ (if there are multiple optimal NPVs, any one can be chosen). By Proposition 6, $\boldsymbol{y}^* = \boldsymbol{A}\,\boldsymbol{x}^* + \boldsymbol{b}$ lies on the surface of $\mathcal{Y}$. Hence, the quest for an optimal strategy can be restricted only to those simple networks that correspond to the triangles on the surface of $\mathcal{Y}$. This observation leads to Algorithm 2, which gives an optimal node prioritization strategy.

Computational complexity of Node Prioritization via Geometric Methods (NPGM): In Algorithm 2, the complexity of Line 1 is $O(n)$. The complexity of Line 2 is $O(n \log n)$ using an optimal output-sensitive algorithm [41] to generate convex hulls. Note that the cardinality of the set $\mathcal{K}$ is no greater than $(6n - 12)$ according to Proposition 9. Hence, the complexity for Line 3 is $O(n)$ since triangulating a convex polygon with n_v vertices can be completed with complexity $O(n_v)$ [42]. Moreover, there are no more than $6n$ cycles in the iteration from Line 4 to Line 13 and each cycle can be completed with complexity $O(1)$, implying that the complexity of the iteration is $O(n)$. Hence, the total computational complexity is $O(n \log n)$.

Proposition 9: Consider a triangulation for the faces of $\mathcal{Y}$ and let $\mathcal{K}$ denote the set consisting of all the resulting triangles. Then $|\mathcal{K}| \leq 6n - 12$.

Proof: Let E denote the number of edges of $\mathcal{Y}$. Then $E \leq 3n - 6$ by Euler's formula. Let l_1, l_2, ..., l_F denote the number of edges for the faces of $\mathcal{Y}$, where F is the number of faces of $\mathcal{Y}$. Then

$$\sum_{k=1}^{F} l_k = 2 \cdot E \leq 6n - 12.$$

Note that a convex polygon with n_{e} edges can be divided into $(n_{\mathrm{e}} - 2)$ triangles. Hence,

$$|\mathcal{K}| \leq \sum_{k=1}^{F} l_k \leq 6n - 12$$

which gives the desired result. $\qquad\square$

C. Visibility-Inspired Approaches

More geometric properties can be exploited to further reduce the candidate set $\mathcal{K}$ in NPGM. Intuitively, $\boldsymbol{A}\,\boldsymbol{x}^* + \boldsymbol{b}$ belongs to the triangle facing the hyperboloid of (8) (the red faces in Fig. 5). To formalize this claim, the definition of visibility is given as follows.

Definition 1 [42]: Given a convex polyhedron $\mathcal{C}$ and a point p outside $\mathcal{C}$. Let h_f denote the open half space that is generated by the plane containing a face f of $\mathcal{C}$ and does not contain $\mathcal{C}$. Then f is *visible* from the point p if p belongs to h_f.

Consider a point $\boldsymbol{y}_\mu = [\,0,\, 0,\, \mu\,]^{\mathrm{T}}$ (μ is an arbitrary negative number). The next proposition shows that $\boldsymbol{y}^*$ lies in a face that is not visible from $\boldsymbol{y}_\mu$.

Proposition 10: $\mathcal{Y}$ has a face f^* that is not visible from $\boldsymbol{y}_\mu$ and contains $\boldsymbol{y}^*$.
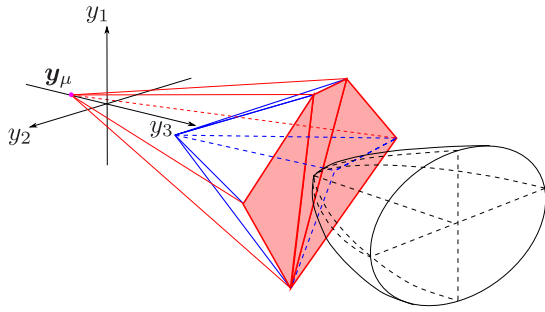
Proof: See Appendix VI. $\qquad\square$

Fig. 5. Illustration of visibility. For the optimal NPV $\boldsymbol{x}^*$, $\boldsymbol{A}\,\boldsymbol{x}^*$ lies in the red faces, which is not visible from $\boldsymbol{y}_\mu$.

Algorithm 3 Node Prioritization Inspired by Visibility (NPIV)

Input: ξ_k and ϕ_k, $k \in \mathcal{N}_\mathrm{b}$

Output: Optimal NPV $\boldsymbol{x}^*$ for $\mathscr{P}_0$

1: Initialization: $\boldsymbol{y}_\mu \leftarrow (\,0, 0, \mu\,)$ where $\mu < 0$ and $|\mu|$ is sufficiently large; $\boldsymbol{x}^* \leftarrow \mathbf{1}/n$ and $\mathcal{P}_\mathrm{tmp} \leftarrow \mathcal{P}(\mathbf{1}/n)$;
2: Construct $\widetilde{\mathcal{Y}} = \mathbb{H}_\mathrm{c}\{\boldsymbol{y}_\mu, \boldsymbol{A}\,\boldsymbol{e} + \boldsymbol{b} : \boldsymbol{e} \in \mathcal{E}\}$;
3: Find a triangulation for the faces of $\widetilde{\mathcal{Y}}$ that do not contain the point $\boldsymbol{y}_\mu$ and let $\widetilde{\mathcal{K}}$ denote the set consisted of all the resulting triangles;
4: **repeat**
5:   Find an element $K_i \in \widetilde{\mathcal{K}}$ and let $\boldsymbol{A}\,\boldsymbol{e}_{i_1} + \boldsymbol{b}$, $\boldsymbol{A}\,\boldsymbol{e}_{i_2} + \boldsymbol{b}$ and $\boldsymbol{A}\,\boldsymbol{e}_{i_3} + \boldsymbol{b}$ denote the vertices of K_i;
6:   Find the optimal NPV $\boldsymbol{x}_\mathrm{tmp}$ according to Proposition 8 and Algorithm 1 for the simple network $\{i_1, i_2, i_3\}$;
7:   **if** $\mathcal{P}(\boldsymbol{x}_\mathrm{tmp}) \leq \mathcal{P}_\mathrm{tmp}$ **then**
8:     $\mathcal{P}_\mathrm{tmp} \leftarrow \mathcal{P}(\boldsymbol{x}_\mathrm{tmp})$;
9:     $\boldsymbol{x}^* \leftarrow \boldsymbol{x}_\mathrm{tmp}$;
10:   **end if**
11:   $\widetilde{\mathcal{K}} \leftarrow \widetilde{\mathcal{K}} \setminus \{K_i\}$;
12: **until** $\widetilde{\mathcal{K}} = \varnothing$
13: Output $\boldsymbol{x}^*$.

The next proposition shows that $\boldsymbol{y}^*$ lies on the surface of $\widetilde{\mathcal{Y}}$, where $\widetilde{\mathcal{Y}}$ is obtained by generating the convex hull of $\boldsymbol{y}_\mu$ and $\mathcal{Y}$.

Proposition 11: f^* stated in Proposition 10 is a face of $\widetilde{\mathcal{Y}}$, where $\widetilde{\mathcal{Y}} = \mathbb{H}_\mathrm{c}\{\boldsymbol{y}_\mu, \boldsymbol{A}\,\boldsymbol{e} + \boldsymbol{b} : \boldsymbol{e} \in \mathcal{E}\}$.

Proof: Since f^* is not visible from $\boldsymbol{y}_\mu$, f^* lies on the surface of the new convex hull generated by the old convex hull $\mathcal{Y}$ and the new point $\boldsymbol{y}_\mu$ [42]. □

Remark 8: Proposition 11 implies that the quest for an optimal strategy can be performed on simple networks corresponding to the triangles on the surface of $\widetilde{\mathcal{Y}}$. Moreover, the search can be limited to the faces that do not contain $\boldsymbol{y}_\mu$ since $\boldsymbol{y}_\mu$ is not in f^*. These observations lead to Algorithm 3, which gives a more efficient and optimal node prioritization strategy.

D. Discussion on Computational Complexity

Regardless of the specific methodology (based either on geometry or on KKT conditions), the node prioritization strategies for simple networks shown in Section IV-A can be naturally extended to networks of arbitrary size based on the sparsity property. In particular, for a network of size n, there are $\binom{n}{3}$ ways to select three out of n anchors. Each
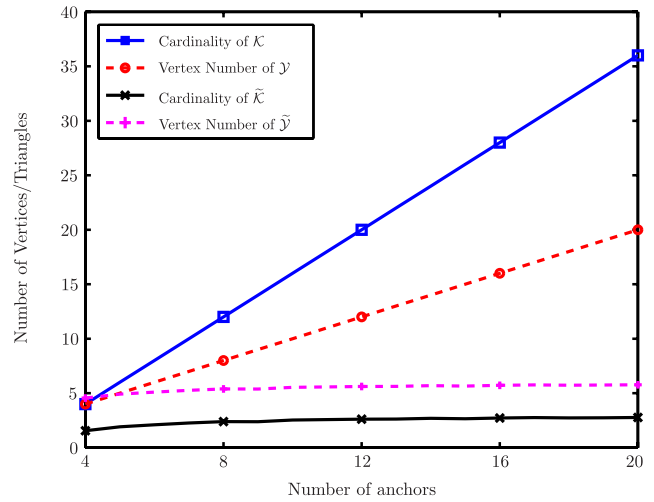

Fig. 6. Vertex number of $\mathcal{Y}$ and $\widetilde{\mathcal{Y}}$ and cardinality of $\mathcal{K}$ and $\widetilde{\mathcal{K}}$.

combination forms a simple network, the optimal solution of which can be obtained efficiently using Algorithm 1. The optimal solution for the entire network can then be obtained by selecting the one with the minimum SPEB among all $\binom{n}{3}$ simple networks. This requires the evaluation of the SPEB for every simple network and its complexity is $O(n^3)$. Comparatively, other strategies that obtain ϵ-approximate solutions using optimization packages (e.g., the SDP and SOCP formulation) have the worst-case complexity $O(n^{3.5})$ [43].

The insight obtained from geometric methods results in NPGM, which enables the reduction of complexity to $O(n \log n)$ without loss of optimality. Moreover, exploiting more geometric properties gives NPIV. Note that NPIV has lower computational complexity than NPGM due to the following reason. The complexity of generating the convex hull is $O(n \log h)$, where h is the number of vertices in the output convex hull [41]. In NPGM, h is equal to n; whereas in NPIV, h is much smaller than n since many vertices of $\mathcal{Y}$ become interior points of $\widetilde{\mathcal{Y}}$. Moreover, the number of iterations from Line 4 to Line 13 decreases significantly since the search in NPIV is limited to faces of $\widetilde{\mathcal{Y}}$ that do not contain $\boldsymbol{y}_\mu$. Fig. 6 shows the number of vertices of the output convex hulls $\mathcal{Y}$ and $\widetilde{\mathcal{Y}}$, and the cardinality of the triangle sets $\mathcal{K}$ and $\widetilde{\mathcal{K}}$ (i.e., the number of cycles from Line 4 to Line 13) as a function of the number of anchors.[6] It can be observed that both the number of vertices of $\mathcal{Y}$ and the cardinality of $\mathcal{K}$ increase linearly with respect to n. Moreover, the number of vertices of $\widetilde{\mathcal{Y}}$ and the cardinality of $\widetilde{\mathcal{K}}$ almost remain a constant as n increases. Such an observation demonstrates the reason for the efficiency improvement of NPIV.

V. NODE PRIORITIZATION WITH INDIVIDUAL CONSTRAINTS

This section provides the optimal strategies for the node prioritization problem with the individual constraint (5).

---

[6]Consider that an agent and a set of anchors are placed randomly in the square region with uniform distribution. The scenario is the same as the one used by Case 1, in Section VII-B.

A. Dimension Augmentation and Projection

Denote the feasible NPV set and its image set, respectively, by

$$\mathcal{X}_{\mathrm{I}} = \{\boldsymbol{x} \in \mathbb{R}^n : \mathbf{1}^{\mathrm{T}} \boldsymbol{x} = 1, \mathbf{0} \preceq \boldsymbol{x} \preceq \boldsymbol{x}^{\mathrm{max}}\}$$

and

$$\mathcal{Y}_{\mathrm{e}} = \{\boldsymbol{y} \in \mathbb{R}^3 : \boldsymbol{y} = \boldsymbol{A}\boldsymbol{x} + \boldsymbol{b}, \boldsymbol{x} \in \mathcal{X}_{\mathrm{I}}\}. \tag{17}$$

For $k \in \mathcal{N}_{\mathrm{b}}$, x_k has two boundary constraints $x_k \geq 0$ and $x_k \leq x_k^{\mathrm{max}}$, where x_k^{max} is the kth element of $\boldsymbol{x}^{\mathrm{max}}$. Note that each element $\boldsymbol{x} \in \mathcal{X}_{\mathrm{I}}$ can be written as a convex combination of elements in

$$\mathcal{E}_{\mathrm{I}} := \{\boldsymbol{x} \in \mathbb{R}^n : \mathbf{1}^{\mathrm{T}} \boldsymbol{x} = 1 \text{ and at least } (n-1)$$
$$\text{boundary constraints are active}\}.$$

Similarly to Proposition 5, the next proposition provides a geometric property of $\mathcal{Y}_{\mathrm{e}}$.

Proposition 12: The image set $\mathcal{Y}_{\mathrm{e}}$ is a convex polyhedron, given by $\mathbb{H}_{\mathrm{c}}\{\boldsymbol{A}\boldsymbol{e} + \boldsymbol{b} : \boldsymbol{e} \in \mathcal{E}_{\mathrm{I}}\}$.

Proposition 12 can be proved similarly to Proposition 5. One can also verify that if $\boldsymbol{x}^*$ is the optimal solution for $\mathscr{P}$, then the image point $\boldsymbol{A}\boldsymbol{x}^* + \boldsymbol{b}$ lies on the surface of $\mathcal{Y}_{\mathrm{e}}$. Therefore, the quest for the optimal strategy of $\mathscr{P}$ can be restricted to the NPVs whose image points lie on the surface of $\mathcal{Y}_{\mathrm{e}}$. However, the complexity of determining the surface of $\mathcal{Y}_{\mathrm{e}}$ via generating the convex hull of $\{\boldsymbol{A}\boldsymbol{e} + \boldsymbol{b} : \boldsymbol{e} \in \mathcal{E}_{\mathrm{I}}\}$ is exponential with respect to n because $\mathcal{E}_{\mathrm{I}}$ can have $O(n \cdot 2^{n-1})$ vertices. Hence, an efficient method to determine $\mathcal{Y}_{\mathrm{e}}$ is required.

Consider a new affine transformation that maps an NPV $\boldsymbol{x}$ to a point in a four-dimensional space, given by

$$\boldsymbol{y}_{\mathrm{e}} = \boldsymbol{A}_{\mathrm{e}}\boldsymbol{x} + \boldsymbol{b}_{\mathrm{e}}$$

where

$$\boldsymbol{A}_{\mathrm{e}} = \begin{bmatrix} \boldsymbol{A} \\ \mathbf{1}_n^{\mathrm{T}} \end{bmatrix} \text{ and } \boldsymbol{b}_{\mathrm{e}} = \begin{bmatrix} \boldsymbol{b} \\ 0 \end{bmatrix}.$$

Note that $\mathcal{Y}_{\mathrm{e}}$ in (17) can be written as

$$\mathcal{Y}_{\mathrm{e}} = \left\{ \boldsymbol{y} : \begin{bmatrix} \boldsymbol{y} \\ y_0 \end{bmatrix} = \begin{bmatrix} \boldsymbol{A}\boldsymbol{x} + \boldsymbol{b} \\ \mathbf{1}^{\mathrm{T}}\boldsymbol{x} \end{bmatrix}, \boldsymbol{x} \in \mathcal{X}_{\mathrm{I}} \right\}$$
$$= \left\{ \boldsymbol{y} : \begin{bmatrix} \boldsymbol{y} \\ y_0 \end{bmatrix} = [\boldsymbol{A}_{\mathrm{e}}\boldsymbol{x} + \boldsymbol{b}_{\mathrm{e}}], y_0 = 1, \mathbf{0} \preceq \boldsymbol{x} \preceq \boldsymbol{x}^{\mathrm{max}} \right\}$$
$$= \left\{ \boldsymbol{y} : \begin{bmatrix} \boldsymbol{y} \\ y_0 \end{bmatrix} \in \mathcal{X}_{\mathrm{F}} \cap \mathcal{Y}_{\mathrm{F}} \right\}$$

where

$$\mathcal{X}_{\mathrm{F}} = \{\boldsymbol{A}_{\mathrm{e}}\boldsymbol{x} + \boldsymbol{b}_{\mathrm{e}} : \mathbf{0} \preceq \boldsymbol{x} \preceq \boldsymbol{x}^{\mathrm{max}}\} \tag{18}$$
$$\mathcal{Y}_{\mathrm{F}} = \left\{ \begin{bmatrix} \boldsymbol{y} \\ 1 \end{bmatrix} : \boldsymbol{y} \in \mathbb{R}^3 \right\}.$$

The relationship among $\mathcal{Y}_{\mathrm{e}}$, $\mathcal{X}_{\mathrm{F}}$ and $\mathcal{Y}_{\mathrm{F}}$ is illustrated with a three-dimensional example in Fig. 7.

Such an observation provides an alternative way to determine the surface of $\mathcal{Y}_{\mathrm{e}}$: one can first generate $\mathcal{X}_{\mathrm{F}}$ and intersect it with $\mathcal{Y}_{\mathrm{F}}$; the resulting polytope is a 3-facet, whose projection onto $\mathbb{R}^3$ is $\mathcal{Y}_{\mathrm{e}}$. Therefore, it is sufficient to determine the edges
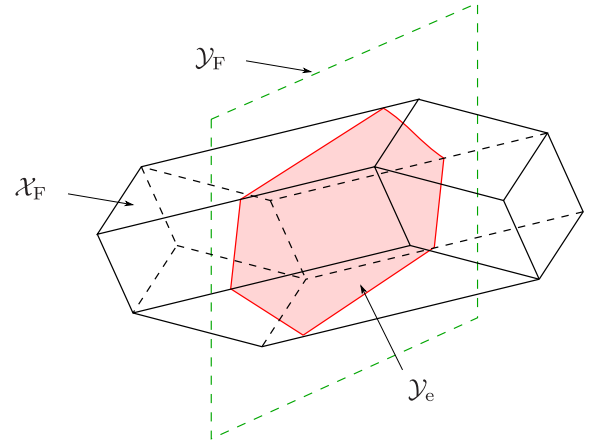

Fig. 7. Illustration of the relationship among $\mathcal{Y}_{\mathrm{e}}$, $\mathcal{X}_{\mathrm{F}}$ and $\mathcal{Y}_{\mathrm{F}}$. $\mathcal{Y}_{\mathrm{e}}$ (red part) is the projection of $\mathcal{X}_{\mathrm{F}} \cap \mathcal{Y}_{\mathrm{F}}$ onto $\mathbb{R}^3$.

of $\mathcal{X}_{\mathrm{F}}$ in order to determine $\mathcal{Y}_{\mathrm{e}}$. Note that $\mathcal{X}_{\mathrm{F}}$ in (18) can be written as

$$\mathcal{X}_{\mathrm{F}} = \left\{ \left(\sum_{k=1}^{n} x_k \boldsymbol{\alpha}_k \right) + \boldsymbol{b}_{\mathrm{e}}, 0 \leq x_k \leq x_k^{\mathrm{max}} \right\}$$
$$= \left\{ \boldsymbol{z} + \boldsymbol{b}_{\mathrm{e}} : \boldsymbol{z} = \sum_{k=1}^{n} x_k \boldsymbol{\alpha}_k, 0 \leq x_k \leq x_k^{\mathrm{max}} \right\}$$

where $\boldsymbol{\alpha}_k = [\xi_k \cos 2\phi_k \ \ \xi_k \sin 2\phi_k \ \ \xi_k \ \ 1]^{\mathrm{T}}$. The edges of $\mathcal{X}_{\mathrm{F}}$ can be determined by solving the LCVBC problem, shown as follows.

B. LCVBC Problem

LCVBC Problem: Given N vectors $\boldsymbol{y}_1, \boldsymbol{y}_2, \ldots, \boldsymbol{y}_N \in \mathbb{R}^d$, the goal is to determine the vertices and edges of the polytope $\mathcal{Y}_{\mathrm{B}}$, given by $\mathcal{Y}_{\mathrm{B}} = \left\{ \sum_{k=1}^{N} c_k \boldsymbol{y}_k : 0 \leq c_k \leq 1 \right\}$.

Without loss of generality, we assume that vectors $\boldsymbol{y}_1$, $\boldsymbol{y}_2, \ldots, \boldsymbol{y}_N$ are not parallel to each other. It can be shown that any vertex $\boldsymbol{y}$ of $\mathcal{Y}_{\mathrm{B}}$ can be written as $\boldsymbol{y} = \sum_{i=1}^{N} w_k \boldsymbol{y}_k$, where $w_k \in \{0, 1\}$ is the *weight* for $\boldsymbol{y}_k$. Therefore, determining the edges of $\mathcal{Y}_{\mathrm{B}}$ is equivalent to finding two vertices and their corresponding weights for each edge of $\mathcal{Y}_{\mathrm{B}}$. Let $\mathcal{W} = \left\{ \{w_k\}_{k=1}^{N} : \sum_{i=1}^{N} w_k \boldsymbol{y}_k \text{ is a vertex of } \mathcal{Y}_{\mathrm{B}} \right\}$ denote the weight set whose elements correspond to vertices of $\mathcal{Y}_{\mathrm{B}}$.

1) Two-Dimensional Case ($d = 2$): Without loss of generality, we assume none of vectors $\boldsymbol{y}_1, \boldsymbol{y}_2, \ldots, \boldsymbol{y}_N$ is parallel to the vertical axis. The polytope $\mathcal{Y}_{\mathrm{B}}$ is determined by Algorithm 4. The process can be divided into two major steps: Line 1 to Line 3 determine the relative position of $\mathcal{Y}_{\mathrm{B}}$; Line 4 to Line 6 find the absolute position of $\mathcal{Y}_{\mathrm{B}}$. Fig. 8 provides an illustration of the proposed algorithm. We claim that Algorithm 4 obtains the desired $\mathcal{Y}_{\mathrm{B}}$ and the proof is given in Appendix VII.

2) General Cases ($d > 2$): $\mathcal{Y}_{\mathrm{B}}$ can be determined by induction on d. The base case ($d = 2$) has been solved by Algorithm 4. Built on that, the higher-dimensional cases can be solved. For ease of exposition, the induction method is demonstrated only for $d = 3$.

One can show that each edge of $\mathcal{Y}_{\mathrm{B}}$ is parallel to one of the vectors $\boldsymbol{y}_1, \boldsymbol{y}_2, \ldots, \boldsymbol{y}_N$. We first determine those edges that are parallel to $\boldsymbol{y}_1$ as follows:

Algorithm 4 LCVBC: Two-Dimensional Case

Input: N vectors in $\mathbb{R}^2$: $\boldsymbol{y}_1, \boldsymbol{y}_2, \ldots, \boldsymbol{y}_N$

Output: Vertices and edges of $\mathcal{Y}_{\mathrm{B}}$: for each edge, determine its two vertices and their corresponding weights

1: Find vectors $-\boldsymbol{y}_1, -\boldsymbol{y}_2, \ldots, -\boldsymbol{y}_N$;

2: Label the $2N$ vectors $\boldsymbol{y}_1, -\boldsymbol{y}_1, \boldsymbol{y}_2, -\boldsymbol{y}_2, \ldots, \boldsymbol{y}_N, -\boldsymbol{y}_N$ in a clockwise order, denoted as $\boldsymbol{y}^{(1)}, \boldsymbol{y}^{(2)}, \ldots, \boldsymbol{y}^{(2N)}$;

3: Connect $\boldsymbol{y}^{(1)}, \boldsymbol{y}^{(2)}, \ldots, \boldsymbol{y}^{(2N)}$, resulting in a polygon $\widetilde{\mathcal{Y}}_{\mathrm{B}}$;

4: Among vectors $\boldsymbol{y}_1, \boldsymbol{y}_2, \ldots, \boldsymbol{y}_N$, search the vectors with positive x components;

5: Sum up these vectors to obtain a point, denoted as $\boldsymbol{y}_{\mathrm{R}}$;

6: Translate $\widetilde{\mathcal{Y}}_{\mathrm{B}}$ by $\boldsymbol{y}_{\mathrm{R}} - \widetilde{\boldsymbol{y}}_{\mathrm{R}}$, where $\widetilde{\boldsymbol{y}}_{\mathrm{R}}$ denotes the rightmost vertex of $\widetilde{\mathcal{Y}}_{\mathrm{B}}$;

7: Output the vertices and the edges of the resulting polygon.

Fig. 9. Illustration of LCVBC in three-dimensional space: $N = 4$.

C. Optimal Strategy Design

Note that 1) the quest for the optimal strategy of $\mathscr{P}$ can be restricted to the strategies corresponding to the surface of $\mathcal{Y}_{\mathrm{e}}$ and 2) the solutions for the LCVBC problem provides an efficient method to determine the triangles on the surface of $\mathcal{Y}_{\mathrm{e}}$. These observations lead to Algorithm 6, which gives an optimal node prioritization strategy for $\mathscr{P}$. The design of Algorithm 6 can be divided into two major parts: Line 2 to Line 5 determine the triangles on the surface of $\mathcal{Y}_{\mathrm{e}}$; Line 6 to Line 14 select the strategy corresponding to the triangles on the surface of $\mathcal{Y}_{\mathrm{e}}$ with the minimum SPEB. In particular, Line 8 determines the optimal node prioritization strategy corresponding to a triangle on the surface of $\mathcal{Y}_{\mathrm{e}}$, which is solved in Section IV.[7]

Computational Complexity of Node Prioritization with Individual Constraints (NPIC): The complexity of Line 1 is $O(n)$. The complexity of Line 2 and Line 3 is $O(n^3 \log n)$ by calling Algorithm 5. Note that $\mathcal{Y}_{\mathrm{e}}$ has $O(n^3)$ edges and $O(n^3)$ vertices. Hence, the complexities for Line 4 and Line 5 are $O(n^3 \log n)$ and $O(n^3)$, respectively. Moreover, there are no more than $O(n^3)$ cycles in the iteration from Line 6 to Line 14 and each cycle has complexity $O(1)$, implying that the complexity of the iteration is $O(n^3)$. Consequently, the total complexity is $O(n^3 \log n)$.

VI. DISCUSSION

This section presents the discussions on several related issues: (i) robust formulation; (ii) exact SPEB with prior knowledge; and (iii) other node prioritization strategies.

A. Robust Formulation

The design of node prioritization strategies is determined by the network parameters, which cannot always be perfectly estimated. The estimated values are subject to uncertainties, and the use of these values may result in suboptimal solutions. Hence, it is necessary to construct robust formulations
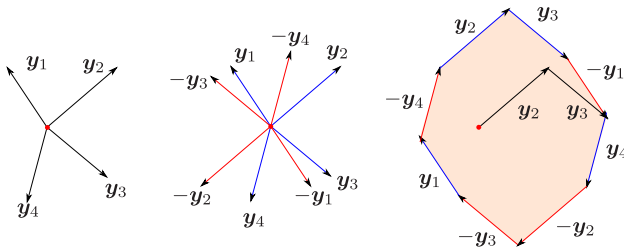

Fig. 8. Illustration of LCVBC in a two-dimensional space. The original vectors are $\boldsymbol{y}_1$ to $\boldsymbol{y}_4$. First find the inverse-vectors, i.e., $-\boldsymbol{y}_1$ to $-\boldsymbol{y}_4$, and then sort all the vectors in a clockwise order. In this case, the order is $(\boldsymbol{y}_1, -\boldsymbol{y}_4, \boldsymbol{y}_2, \boldsymbol{y}_3, -\boldsymbol{y}_1, \boldsymbol{y}_4, -\boldsymbol{y}_2, -\boldsymbol{y}_3)$. Connect the edges (original and inverse ones) in such clockwise order, resulting in a polygon $\widetilde{\mathcal{Y}}_{\mathrm{B}}$. The vectors with positive x-components are $\boldsymbol{y}_2$ and $\boldsymbol{y}_3$, so $\boldsymbol{y}_{\mathrm{R}} = \boldsymbol{y}_2 + \boldsymbol{y}_3$.

- Generate a normal plane $\mathcal{Y}_{\mathrm{n}}^1$ of vector $\boldsymbol{y}_1$;
- Project vectors $\boldsymbol{y}_2$ to $\boldsymbol{y}_N$ onto $\mathcal{Y}_{\mathrm{n}}^1$, resulting in $N-1$ vectors in a two-dimensional space, denoted as $\boldsymbol{z}_2^1, \boldsymbol{z}_3^1, \ldots, \boldsymbol{z}_N^1$;
- For these $N-1$ vectors in the two-dimensional space, solve the LCVBC problem by Algorithm 4 and determine the weight set $\mathcal{W}_1$ for the vertices of the resulting polygon, denoted as $\mathcal{Y}_{\mathrm{B,n}}^1$;
- For any weight $[w_2^1 \ w_3^1 \ \ldots \ w_N^1] \in \mathcal{W}_1$, the segment $\left\{ \sum_{k=2}^N w_k^1 \boldsymbol{y}_k + t \cdot \boldsymbol{y}_1, 0 \le t \le 1 \right\}$, parallel to $\boldsymbol{y}_1$, is an edge of $\mathcal{Y}_{\mathrm{B}}$. All the edges of $\mathcal{Y}_{\mathrm{B}}$ that are parallel to $\boldsymbol{y}_1$ can be found in this way due to the following lemma.

Lemma 1: If an edge e of $\mathcal{Y}_{\mathrm{B}}$ is parallel to $\boldsymbol{y}_1$, then the projection of e onto $\mathcal{Y}_{\mathrm{n}}^1$ is a vertex of $\mathcal{Y}_{\mathrm{B,n}}^1$; if v is a vertex of $\mathcal{Y}_{\mathrm{B,n}}^1$, then $\mathcal{Y}_{\mathrm{B}}$ has an edge e such that e is parallel to $\boldsymbol{y}_1$ and the projection of e onto $\mathcal{Y}_{\mathrm{n}}^1$ is v.

The proof of Lemma 1 is straightforward and omitted for brevity. Fig. 9 provides an illustration of the steps above. Following a similar process, one can obtain the edges of $\mathcal{Y}_{\mathrm{B}}$ that are parallel to $\boldsymbol{y}_2, \boldsymbol{y}_3, \ldots, \boldsymbol{y}_N$, and in this way, all the edges of $\mathcal{Y}_{\mathrm{B}}$ can be determined. Details of the procedure are given in Algorithm 5. One can verify that the complexities are $O(N \log N)$ and $O(N^{d-1} \log N)$ for Algorithm 4 and Algorithm 5, respectively.
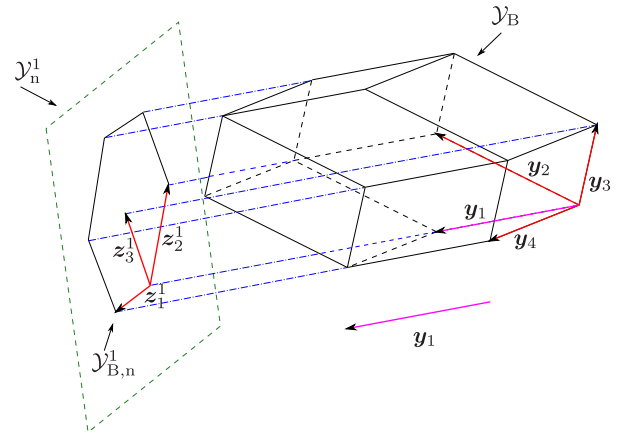
---

[7]Note that in Section IV-A, we formulate the problem of $\mathscr{P}_{\mathrm{S}}$ for general NPVs $\boldsymbol{x}_k$ ($k = 1, 2, 3$) without assuming the structure of $\boldsymbol{x}_k$, and therefore, the proposed geometric solution to the problem of $\mathscr{P}_{\mathrm{S}}$ in Section IV-A provides the optimal node prioritization strategy corresponding to a particular triangle on the surface of $\mathcal{Y}_{\mathrm{e}}$.

Algorithm 5 LCVBC: General Cases

Input: N vectors in $\mathbb{R}^d$ with $d > 2$: $\boldsymbol{y}_1, \boldsymbol{y}_2, \ldots, \boldsymbol{y}_N$

Output: Vertices and edges of $\mathcal{Y}_{\mathrm{B}}$: for each edge, determine its two vertices and their corresponding weights

1: Initialization: $k = 1$;
2: **while** $k \leq N$ **do**
3:     Generate a normal $(d-1)$-plane $\mathcal{Y}_{\mathrm{n}}^k$ of $\boldsymbol{y}_k$;
4:     Project vectors $\boldsymbol{y}_1, \boldsymbol{y}_2, \ldots, \boldsymbol{y}_{k-1}, \boldsymbol{y}_{k+1}, \ldots, \boldsymbol{y}_N$ onto $\mathcal{Y}_{\mathrm{n}}^k$, resulting $N-1$ vectors in a $(d-1)$-dimensional space, denoted as $\boldsymbol{z}_1^k, \boldsymbol{z}_2^k, \ldots, \boldsymbol{z}_{k-1}^k, \boldsymbol{z}_{k+1}^k, \ldots, \boldsymbol{z}_N^k$;
5:     **if** $d = 3$ **then**
6:         Call Algorithm 4 with input $\boldsymbol{z}_1^k, \boldsymbol{z}_2^k, \ldots, \boldsymbol{z}_{k-1}^k, \boldsymbol{z}_{k+1}^k, \ldots, \boldsymbol{z}_N^k$;
7:         Record the weight set $\mathcal{W}_k$ for the vertices of the resulting polygon;
8:     **else**
9:         Call Algorithm 5 with input $\boldsymbol{z}_1^k, \boldsymbol{z}_2^k, \ldots, \boldsymbol{z}_{k-1}^k, \boldsymbol{z}_{k+1}^k, \ldots, \boldsymbol{z}_N^k$;
10:        Record the weight set $\mathcal{W}_k$ for the vertices of the resulting polytope;
11:     **end if**
12:     **repeat**
13:         Find $[\, w_1^k \; w_2^k \; \ldots \; w_{k-1}^k \; w_{k+1}^k \; \ldots \; w_N^k \,] \in \mathcal{W}_k$;
14:         Add the following segment to the edge set of $\mathcal{Y}_{\mathrm{B}}$

$$\left\{ \sum_{1 \leq j \leq N, j \neq k} w_j^k \boldsymbol{y}_j + t \cdot \boldsymbol{y}_k, 0 \leq t \leq 1 \right\}$$

15:         $\mathcal{W}_k \leftarrow \mathcal{W}_k \setminus [\, w_1^k \; w_2^k \; \ldots \; w_{k-1}^k \; w_{k+1}^k \; \ldots \; w_N^k \,]$;
16:     **until** $\mathcal{W}_k = \varnothing$;
17:     $k \leftarrow k + 1$;
18: **end while**

---

accounting for the parameter uncertainties. We consider that $\xi_k \in \mathcal{S}_k^\xi$ and $\phi_k \in \mathcal{S}_k^\phi$, where

$$\mathcal{S}_k^\xi := \left[\, \hat{\xi}_k - \epsilon_k^\xi, \hat{\xi}_k + \epsilon_k^\xi \,\right] = \left[\, \underline{\xi}_k, \overline{\xi}_k \,\right]$$
$$\mathcal{S}_k^\phi := \left[\, \hat{\phi}_k - \epsilon_k^\phi, \hat{\phi}_k + \epsilon_k^\phi \,\right] = \left[\, \underline{\phi}_k, \overline{\phi}_k \,\right]$$

in which $\hat{\xi}_k$ and $\hat{\phi}_k$ denote the nominal values of the ERC and angles; ϵ_k^ξ and ϵ_k^ϕ denote ERC and angle uncertainties.[8] In this setting, the worst-case SPEB is given by

$$\mathcal{P}_{\mathrm{R}}(\boldsymbol{x}) = \max_{\xi_k \in \mathcal{S}_k^\xi, \phi_k \in \mathcal{S}_k^\phi} \mathcal{P}(\boldsymbol{x}) = \max_{\xi_k = \underline{\xi}_k, \phi_k \in \mathcal{S}_k^\phi} \mathcal{P}(\boldsymbol{x})$$

where the second equation is due to the fact that the SPEB monotonically decreases in ξ_k.[9]

Direct maximization over ϕ_k is non-trivial. To address this problem, an auxiliary matrix is introduced as

$$\boldsymbol{Q}_{\mathrm{e}}(\boldsymbol{p}_0; \boldsymbol{x}) = \boldsymbol{J}_0 + \sum_{k \in \mathcal{N}_{\mathrm{b}}} \underline{\xi}_k x_k \cdot (\boldsymbol{J}_{\mathrm{r}}(\hat{\phi}_k) - \delta_k \cdot \boldsymbol{I})$$

---

[8] Note that with such constraints, the estimation of $\boldsymbol{p}_0$ becomes a constrained estimation problem. However, the corresponding SPEB is not affected by the constraints since the considered parameters are *regular*, as shown in [44].

[9] The monotonicity of SPEB in ERC can be proved similarly to Proposition 2.

Algorithm 6 Node Prioritization with Individual Constraints (NPIC)

Input: ξ_k and ϕ_k, $k \in \mathcal{N}_{\mathrm{b}}$; $\boldsymbol{x}^{\max} \in \mathbb{R}^n$

Output: Optimal NPV $\boldsymbol{x}^*$ for $\mathscr{P}$

1: Initialization: $\mathcal{P}_{\mathrm{tmp}}$ is assigned to a sufficiently large number;
2: Call Algorithm 5 with inputs $\boldsymbol{y}_k = x_k^{\max} \boldsymbol{A}_{\mathrm{e}} \boldsymbol{e}_k$, $k \in \mathcal{N}_{\mathrm{b}}$, and translate the resulting polytope by $\boldsymbol{b}_{\mathrm{e}}$, providing $\mathcal{X}_{\mathrm{F}}$;
3: Intersect $\mathcal{X}_{\mathrm{F}}$ with $\mathcal{Y}_{\mathrm{F}}$ and project the results onto $\mathbb{R}^3$ to obtain the vertices of $\mathcal{Y}_{\mathrm{e}}$;
4: Generate the convex hull for the vertices of $\mathcal{Y}_{\mathrm{e}}$;
5: Find a triangulation for the faces of $\mathcal{Y}_{\mathrm{e}}$ and let $\mathcal{K}$ denote the set consisted of all the resulting triangles;
6: **repeat**
7:     Find an element $K_i \in \mathcal{K}$;
8:     Find the optimal NPV $\boldsymbol{x}_{\mathrm{tmp}}$ corresponding to K_i based on the solution for $\mathscr{P}_{\mathrm{S}}$;
9:     **if** $\mathcal{P}(\boldsymbol{x}_{\mathrm{tmp}}) \leq \mathcal{P}_{\mathrm{tmp}}$ **then**
10:        $\mathcal{P}_{\mathrm{tmp}} \leftarrow \mathcal{P}(\boldsymbol{x}_{\mathrm{tmp}})$;
11:        $\boldsymbol{x}^* \leftarrow \boldsymbol{x}_{\mathrm{tmp}}$;
12:     **end if**
13:     $\mathcal{K} \leftarrow \mathcal{K} \setminus \{K_i\}$;
14: **until** $\mathcal{K} = \varnothing$
15: Output $\boldsymbol{x}^*$.

---

where $\delta_k = |\sin \epsilon_k^\phi|$. It has been shown in [32] that for any $\phi_k \in \mathcal{S}_k^\phi$, $\xi_k \in \mathcal{S}_k^\xi$,

$$\boldsymbol{Q}_{\mathrm{e}}(\boldsymbol{p}_0; \boldsymbol{x}) \preceq \boldsymbol{J}_{\mathrm{e}}(\boldsymbol{p}_0; \boldsymbol{x})$$

and consequently,

$$\overline{\mathcal{P}}_{\mathrm{R}}(\boldsymbol{x}) := \mathrm{tr}\big\{ \boldsymbol{Q}_{\mathrm{e}}^{-1}(\boldsymbol{p}_0; \boldsymbol{x}) \big\} \geq \mathrm{tr}\big\{ \boldsymbol{J}_{\mathrm{e}}^{-1}(\boldsymbol{p}_0; \boldsymbol{x}) \big\} = \mathcal{P}(\boldsymbol{x})$$

provided that $\boldsymbol{Q}_{\mathrm{e}}(\boldsymbol{p}_0; \boldsymbol{x}) \succeq \boldsymbol{0}$. With this observation, the robust node prioritization problem, denoted as $\mathscr{P}_{\mathrm{R}}$, can be formulated as

$$\mathscr{P}_{\mathrm{R}}: \quad \begin{aligned} \underset{\boldsymbol{x} \in \mathbb{R}^n}{\text{minimize}} \quad & \overline{\mathcal{P}}_{\mathrm{R}}(\boldsymbol{x}) \\ \text{subject to} \quad & \boldsymbol{1}^{\mathrm{T}} \boldsymbol{x} \leq 1 \\ & \boldsymbol{x} \succeq \boldsymbol{0} \\ & \boldsymbol{x} \preceq \boldsymbol{x}^{\max} \\ & \boldsymbol{Q}_{\mathrm{e}}(\boldsymbol{p}_0; \boldsymbol{x}) \succeq \boldsymbol{0}. \end{aligned}$$

Note that $\mathscr{P}_{\mathrm{R}}$ is a convex problem and the optimal solution exists [40]. We next show how to solve $\mathscr{P}_{\mathrm{R}}$ with geometric methods. Consider an affine transformation

$$\boldsymbol{y} = \underline{\boldsymbol{A}} \boldsymbol{x} + \boldsymbol{b}$$

where $\underline{\boldsymbol{A}} = [\, \boldsymbol{c} \; \boldsymbol{s} \; \boldsymbol{1} - 2\boldsymbol{\delta} \,]^{\mathrm{T}} \underline{\boldsymbol{R}}$, in which $\boldsymbol{\delta} = [\, \delta_1 \, \delta_2 \, \ldots \, \delta_n \,]^{\mathrm{T}}$ and $\underline{\boldsymbol{R}} = \mathrm{diag}\{\underline{\xi}_1, \underline{\xi}_2, \ldots, \underline{\xi}_n\}$. Consider the following sets

$$\widetilde{\mathcal{X}}_{\mathrm{I}} = \{\boldsymbol{x} \in \mathbb{R}^n : \boldsymbol{1}^{\mathrm{T}} \boldsymbol{x} \leq 1, \boldsymbol{0} \preceq \boldsymbol{x} \preceq \boldsymbol{x}^{\max}\}$$
$$\widetilde{\mathcal{Y}}_{\mathrm{I}} = \{\boldsymbol{y} \in \mathbb{R}^3 : \boldsymbol{y} = \underline{\boldsymbol{A}} \boldsymbol{x} + \boldsymbol{b}, \boldsymbol{x} \in \widetilde{\mathcal{X}}_{\mathrm{I}}\}.$$

The function $\boldsymbol{Q}_{\mathrm{e}}(\boldsymbol{x})$ may not be an increasing function for $\boldsymbol{x} \succeq \boldsymbol{0}$ and hence we need to consider $\boldsymbol{1}^{\mathrm{T}} \boldsymbol{x} \leq 1$ rather

than $\mathbf{1}^{\mathrm{T}} \boldsymbol{x} = 1$. We have the following counterpart of Proposition 6.

Proposition 13: If $\boldsymbol{x}^*$ is an optimal solution for $\mathscr{P}_{\mathrm{R}}$, then $\boldsymbol{y}^* = \underline{\boldsymbol{A}}\, \boldsymbol{x}^* + \boldsymbol{b}$ lies on the surface of the convex polyhedron $\widetilde{\mathcal{Y}}_{\mathrm{I}}$.

Proof: Let $\widetilde{\mathcal{Y}}_{\mathrm{e}}$ denote the image set of feasible NPVs of $\mathscr{P}_{\mathrm{R}}$. Note that

$$\boldsymbol{Q}_{\mathrm{e}}(\boldsymbol{p}_0; \boldsymbol{x}) \succeq \boldsymbol{0} \Leftrightarrow \begin{bmatrix} (y_3 + y_1)/2 & y_2/2 \\ y_2/2 & (y_3 - y_1)/2 \end{bmatrix} \succeq \boldsymbol{0}$$

$$\Leftrightarrow y_3 \geq |y_1| \text{ and } y_3^2 \geq y_1^2 + y_2^2$$

$$\Leftrightarrow y_3 \geq 0 \quad \text{and } y_3^2 \geq y_1^2 + y_2^2.$$

Then

$$\widetilde{\mathcal{Y}}_{\mathrm{e}} = \widetilde{\mathcal{Y}}_{\mathrm{I}} \cap \left\{ \boldsymbol{y} \in \mathbb{R}^3 : y_3 \geq 0 \text{ and } y_3^2 \geq y_1^2 + y_2^2 \right\}.$$

We first prove that $\boldsymbol{y}^*$ lies on the boundary of $\widetilde{\mathcal{Y}}_{\mathrm{e}}$ by contradiction. Let $\lambda^* = \overline{\mathcal{P}}_{\mathrm{R}}(\boldsymbol{x}^*)$. Suppose $\boldsymbol{y}^*$ is an interior point of $\widetilde{\mathcal{Y}}_{\mathrm{e}}$, then by the definition of interior point, there exists $\epsilon > 0$ such that $\{\boldsymbol{y} : \|\boldsymbol{y} - \boldsymbol{y}^*\| < \epsilon\} \subseteq \widetilde{\mathcal{Y}}_{\mathrm{e}}$. Consider the set

$$\mathcal{Y}_{\lambda^*} = \left\{ \boldsymbol{y} \in \mathbb{R}^3 : y_3 > 0 \text{ and } 0 < \frac{4\, y_3}{y_3^2 - y_1^2 - y_2^2} < \lambda^* \right\}$$

and it can be verified that $\mathcal{Y}_{\lambda^*}$ is an open set and $\boldsymbol{y}^*$ lies on the boundary of $\mathcal{Y}_{\lambda^*}$. Therefore, $\{\boldsymbol{y} : \|\boldsymbol{y} - \boldsymbol{y}^*\| < \epsilon\} \cap \mathcal{Y}_{\lambda^*} \neq \varnothing$. Consequently, $\widetilde{\mathcal{Y}}_{\mathrm{e}} \cap \mathcal{Y}_{\lambda^*} \neq \varnothing$. Let $\boldsymbol{x}_\delta$ denote a feasible NPV such that $\underline{\boldsymbol{A}}\, \boldsymbol{x}_\delta + \boldsymbol{b} \in \widetilde{\mathcal{Y}}_{\mathrm{e}} \cap \mathcal{Y}_{\lambda^*}$. Equation (7) gives

$$0 < \overline{\mathcal{P}}_{\mathrm{R}}(\boldsymbol{x}_\delta) = Q(\underline{\boldsymbol{A}}\, \boldsymbol{x}_\delta + \boldsymbol{b}) < \lambda^*.$$

This is a contradiction since $\boldsymbol{x}^*$ is an optimal solution for $\mathscr{P}_{\mathrm{R}}$.

Note that the boundary of $\widetilde{\mathcal{Y}}_{\mathrm{e}}$ belongs to the union of the surface of $\widetilde{\mathcal{Y}}_{\mathrm{I}}$ and the boundary of

$$\left\{ \boldsymbol{y} \in \mathbb{R}^3 : y_3 \geq 0 \text{ and } y_3^2 \geq y_1^2 + y_2^2 \right\}.$$

However, $\boldsymbol{y}^*$ does not lies on the latter since

$$0 < Q(\boldsymbol{y}^*) = \frac{4 y_3^*}{y_3^{*2} - y_1^{*2} - y_2^{*2}} < \infty.$$

Consequently, $\boldsymbol{y}^*$ lies on the surface of $\widetilde{\mathcal{Y}}_{\mathrm{I}}$, which completes the proof.   □

Proposition 13 implies that the quest for the optimal strategy of $\mathscr{P}_{\mathrm{R}}$ can be restricted to the strategies that correspond to the surface of $\widetilde{\mathcal{Y}}_{\mathrm{I}}$. The geometric methods proposed in Section III to Section V can be used to solve the robust node prioritization problem $\mathscr{P}_{\mathrm{R}}$.[10]

B. Exact SPEB With Prior Knowledge

Recall that in Section II-A, if $\boldsymbol{J}_0 \neq \boldsymbol{0}_{2,2}$, $\boldsymbol{J}_{\mathrm{e}}(\boldsymbol{p}_0; \boldsymbol{x})$ provides an approximation of the FIM and $\mathcal{P}(\boldsymbol{x}) = \mathrm{tr}\{\boldsymbol{J}_{\mathrm{e}}^{-1}(\boldsymbol{p}_0; \boldsymbol{x})\}$ is an approximation of the SPEB. We next show that the geometric methods developed in this paper can be used to solve node prioritization problems that adopt the exact SPEB in the case where $\boldsymbol{J}_0 \neq \boldsymbol{0}_{2,2}$ as the performance metric.

---

[10]Note that in Algorithm 1, the output $\boldsymbol{y}^\circ$ needs to satisfy $y_3^\circ > 0$ and $(y_3^\circ)^2 > (y_1^\circ)^2 + (y_2^\circ)^2$.

Derivation of the exact FIM involves averaging over the prior knowledge and the exact FIM is given by [10]

$$\boldsymbol{J}_{\mathrm{a,e}} = \boldsymbol{J}_0 + \sum_{k \in \mathcal{N}_{\mathrm{b}}} x_k\, \boldsymbol{J}_{\mathrm{a},k}$$

where $\boldsymbol{J}_{\mathrm{a},k} = \mathbb{E}\{\xi_k\, \boldsymbol{J}_{\mathrm{r}}(\varphi_k)\}$, in which the expectation is taken with respect to the joint distribution of the agent's prior positional knowledge and the prior ERC knowledge through ξ_k and φ_k. Consequently, the exact SPEB is

$$\mathcal{P}_{\mathrm{a}}(\boldsymbol{x}) = \mathrm{tr}\{\boldsymbol{J}_{\mathrm{a,e}}^{-1}(\boldsymbol{x})\}.$$

Note that by eigenvalue decomposition, the FIM $\boldsymbol{J}_{\mathrm{a},k}$ can be decomposed as

$$\boldsymbol{J}_{\mathrm{a},k} = \xi_k^{(1)}\, \boldsymbol{J}_{\mathrm{r}}(\varphi_k^{(1)}) + \xi_k^{(2)}\, \boldsymbol{J}_{\mathrm{r}}(\varphi_k^{(2)})$$

where $\xi_k^{(1)}$, $\xi_k^{(2)} \geq 0$ are the eigenvalues of $\boldsymbol{J}_{\mathrm{a},k}$ and $\varphi_k^{(1)}$, $\varphi_k^{(2)} = \varphi_k^{(1)} + \pi/2$ are the angles of the corresponding eigenvectors. Consider an affine transformation

$$\boldsymbol{y} = \boldsymbol{A}_{\mathrm{a}}\, \boldsymbol{x} + \boldsymbol{b}$$

where

$$\boldsymbol{A}_{\mathrm{a}} = [\, \boldsymbol{c}_{\mathrm{a}} \quad \boldsymbol{s}_{\mathrm{a}} \quad \boldsymbol{1} \,]^{\mathrm{T}}\, \boldsymbol{R}^{(1)} - [\, \boldsymbol{c}_{\mathrm{a}} \quad \boldsymbol{s}_{\mathrm{a}} \quad -\boldsymbol{1} \,]^{\mathrm{T}}\, \boldsymbol{R}^{(2)}$$

in which

$$\boldsymbol{R}^{(i)} = \mathrm{diag}\{\xi_1^{(i)}, \xi_2^{(i)}, \ldots, \xi_n^{(i)}\}, \quad i = 1, 2$$

and

$$\boldsymbol{c}_{\mathrm{a}} = \begin{bmatrix} \cos 2\varphi_1^{(1)} & \cos 2\varphi_2^{(1)} & \ldots & \cos 2\varphi_n^{(1)} \end{bmatrix}^{\mathrm{T}}$$
$$\boldsymbol{s}_{\mathrm{a}} = \begin{bmatrix} \sin 2\varphi_1^{(1)} & \sin 2\varphi_2^{(1)} & \ldots & \sin 2\varphi_n^{(1)} \end{bmatrix}^{\mathrm{T}}.$$

With this transformation, the methods proposed in Section III to Section V can be used to solve the node prioritization problem with the exact FIM. Note that the exact SPEB involves the integration over the distribution of the agent's prior knowledge and does not admit a closed-form expression. Hence, the approximate SPEB is more favorable to be used as the performance metric.

C. Heuristic Node Prioritization Strategies

We next propose some heuristic node prioritization strategies in network localization. The performance of these strategies will be evaluated in Section VII.

1) No Individual Constraints: The following three strategies are proposed to solve $\mathscr{P}_0$.

- Uniform Strategy: allocate transmission resources equally among anchors;
- Strategy I: select three anchors corresponding to the largest ERCs and then find the optimal NPV for this simple network;
- Strategy II: divide the anchors $k \in \mathcal{N}_{\mathrm{b}}$ into three groups $\mathcal{G}_1$, $\mathcal{G}_2$, and $\mathcal{G}_3$ in the following way: $k \in \mathcal{G}_1$ if $\phi_k \in [0, 2\pi/3)$; $k \in \mathcal{G}_2$ if $\phi_k \in [2\pi/3, 4\pi/3)$; and $k \in \mathcal{G}_3$ if $\phi_k \in [4\pi/3, 2\pi)$; select the anchor with the maximum ERC in each group; and then find the optimal NPV for this simple network;
- Strategy III: search all $\binom{n}{3}$ simple networks and select the one with the minimum SPEB, proposed in Section IV-D.

Algorithm 7 Strategy IV and V

Input: ξ_k and ϕ_k, $k \in \mathcal{N}_b$; $\boldsymbol{x}^{\max} \in \mathbb{R}^n$
Output: An NPV $\boldsymbol{x}$ for $\mathscr{P}$
1: $\mathcal{U}_c \leftarrow \varnothing$;
2: **repeat**
3:     Determine a solution $\boldsymbol{x}$ of $\mathscr{P}_M$ for given $\mathcal{U}_c$ (either adopting NPIV or Uniform Strategy);
4:     **for** $k \in \mathcal{N}_b \setminus \mathcal{U}_c$ **do**
5:         **if** $x_k > x_k^{\max}$ **then**
6:             $\mathcal{U}_c \leftarrow \mathcal{U}_c \cup \{k\}$;
7:         **end if**
8:     **end for**
9: **until** $\boldsymbol{x} \preceq \boldsymbol{x}_k^{\max}$
10: Output $\boldsymbol{x}$.

TABLE I
COMPUTATIONAL COMPLEXITY FOR STRATEGIES WITH ($\mathscr{P}_0$) AND
WITHOUT ($\mathscr{P}$) INDIVIDUAL CONSTRAINTS

		Optimal		Suboptimal	
	Name	Complexity	Name	Complexity	
	NPGM	$O(n \log n)$	Uniform	$O(1)$	
$\mathscr{P}_0$	NPIV	$O(n \log h)$	Stra. II	$O(n)$	
	Stra. III	$O(n^3)$	Stra. I	$O(n)$	
$\mathscr{P}$	NPIC	$O(n^3 \log n)$	Stra. IV	$O(n^2 \log n)$	
	Stra. VI	$O(n \cdot 2^n)$	Stra. V	$O(n^2)$	

2) With Individual Constraints: The following strategies are proposed to solve $\mathscr{P}$:

- Strategy IV operates in an iterative way and it maintains an *upper bound anchor set* $\mathcal{U}_c$, which contains the indexes of anchors that have violated the individual constraints (5) in the iterations. Details are given in Algorithm 7. Note that in Line 3, Strategy IV adopts NPIV to solve the following problem:

$$\mathscr{P}_M: \quad \underset{\boldsymbol{x} \in \mathbb{R}^n}{\text{minimize}} \quad \mathcal{P}(\boldsymbol{x})$$
$$\text{subject to} \quad \mathbf{1}^T \boldsymbol{x} \leq 1$$
$$x_k = x_k^{\max}, \quad k \in \mathcal{U}_c$$
$$\boldsymbol{x} \succeq \mathbf{0}.$$

- Strategy V follows the same procedure as Strategy IV except that Strategy V adopts Uniform Strategy to solve $\mathscr{P}_M$ in Line 3. Note that there are no more than n cycles in the iteration from Line 4 to Line 9. Hence, the complexities are $O(n^2 \log n)$ and $O(n^2)$ for Strategy IV and V, respectively.
- Strategy VI first finds the triangles on the surface of $\mathcal{Y}_e$ by determining $\mathcal{E}_I$ and $\mathcal{Y}_e = \mathbb{H}_c\{\mathcal{E}_I\}$, and then follows Line 6 to 15 in Algorithm 6 to provide an optimal NPV. One can verify that the complexity of Strategy VI is $O(n \cdot 2^n)$.

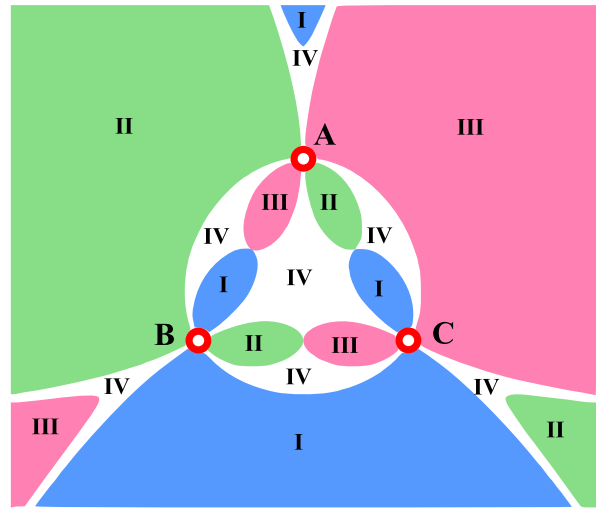The computational complexities of all the proposed strategies are given in Table I.

Fig. 10. The optimal strategy for $\mathscr{P}_0$ uses B and C if the agent is in region I; it uses A and B if the agent is in region II; it uses A and C if the agent is in region III; and it uses A, B and C if the agent is in region IV.

VII. NUMERICAL RESULTS

This section provides numerical results to illustrate the sparsity property of the optimal NPV and the performance of the proposed strategies.

A. Anchor Selection and Sparsity Property

We consider two examples of anchor selection where the agent is located at different positions. Free-space pathloss is used as the signal propagation model.

In Fig. 10, three anchors (A, B and C) are deployed at the vertices of an equilateral triangle. The plane is divided into four types of regions labeled as I, II, III, and IV. The node prioritization strategy that achieves the optimal localization performance requires different sets of anchors corresponding to the agent's position. For instance, the resources are allocated to all the three anchors if the agent is in region IV. First, the area of region IV is relatively small, implying that in most cases only two anchors are required to achieve the optimal localization performance. Second, if the agent is in the "far field" region, i.e., it is sufficiently far away from all the anchors, the optimal strategy for $\mathscr{P}_0$ requires two active anchors. Third, if the agent lies on the line formed by two anchors, the anchor farther to the agent will not be used to achieve the optimal localization performance. This is intuitive since allocating resources to the closer anchor is more efficient for improving the localization performance.

In Fig. 11, seven anchors are deployed at the vertices of a heptagon and nine agents are deployed in nine different positions. The directions of the arrows show the anchors activated for a particular agent. For example, the optimal strategy uses anchors A and B for agent C. The length of the arrow corresponds to the amount of allocated resources. Fig. 11 demonstrates the sparsity property of the optimal NPV. It can be observed that active anchors for an agent depend on the distances and angles between anchors and the agent.
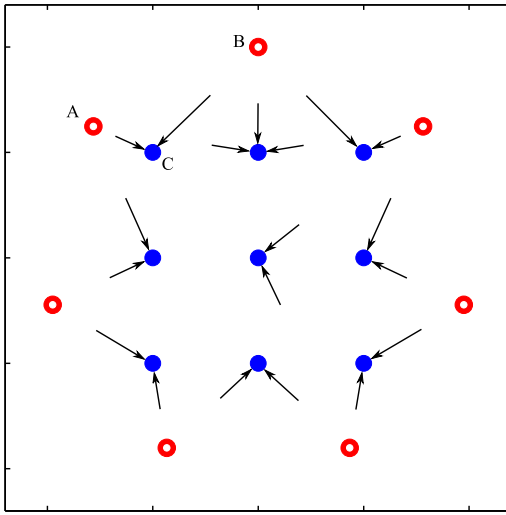
Fig. 11. Illustration of optimal node prioritization with anchors deployed at the vertices of a heptagon.

Fig. 13. Average SPEB as a function of the number of anchors for the optimal strategy, Strategy I, Strategy II and Uniform Strategy with prior positional knowledge.
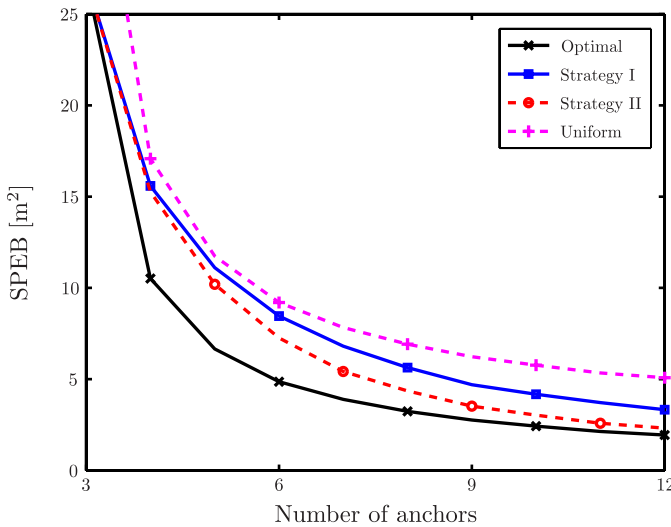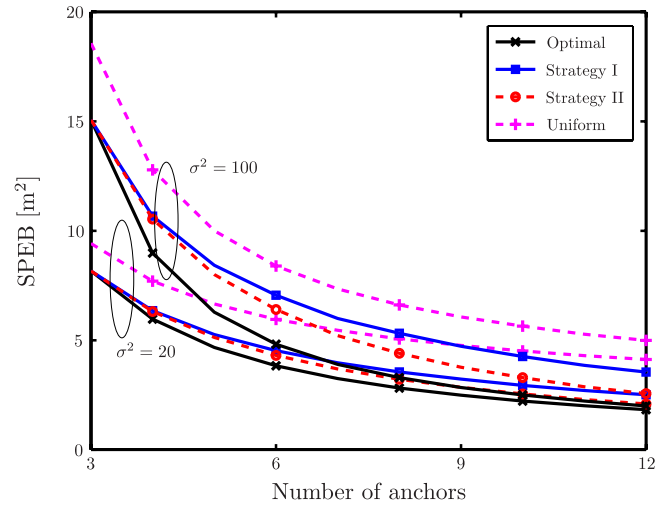

Fig. 12. Average SPEB as a function of the number of anchors for the optimal strategy, Strategy I, Strategy II, and Uniform Strategy without prior positional knowledge.

B. Performance of Node Prioritization Strategies

In this section, consider that $\boldsymbol{x}$ is the NPV based on power (with power unit Watt) as in Appendix I-A. The simulation is carried out in a two-dimensional network where an agent and a set of anchors are placed randomly in a square region (100 m × 100 m) with a uniform distribution. Consider that $\{\xi_k d_k^2\}_{k \in \mathcal{N}_b}$ are modeled as independent Rayleigh random variables with mean 6.3×10^3.[11]

Case 1) No Prior Knowledge, No Individual Constraints: The performance of the optimal strategy and three other efficient strategies (i.e., Uniform Strategy, Strategy I and Strategy II) are compared. Fig. 12 shows the SPEB as a function of the number of anchors for different strategies.

---

[11]The mean of the Rayleigh random variable is obtained based on the following choice of parameters: carrier frequency 5 GHz, bandwidth 500 MHz and $\beta = 1$. Moreover, the Extended Typical Urban model is used for the power dispersion profile [45]. The unit of the random variable is $(\text{Watt})^{-1}$.

First, the achieved SPEB decreases with the number of anchors for each strategy since more anchors provide more degrees of freedom, resulting in a higher diversity gain. Second, the optimal strategy outperforms all the heuristic strategies, e.g., reducing the SPEB by more than 50%, 40%, and 20% compared to Uniform Strategy, Strategy I and Strategy II, respectively, when $n = 10$. Third, Strategy II outperforms Strategy I, and they both perform better than Uniform Strategy. This agrees with intuition because Strategy II accounts for the effects of both angles and ERCs while Strategy I considers only ERCs.

Case 2) Prior Knowledge, No Individual Constraints: The performances of the optimal strategy and three efficient strategies (i.e., Uniform Strategy, Strategy I and Strategy II) are compared. The prior positional knowledge of the agent follows a Gaussian distribution $\mathcal{N}(\boldsymbol{p}_0, \sigma^2 \boldsymbol{I}_2)$, where σ is the standard deviation of the prior position distribution with the unit m. Fig. 13 shows the SPEB as a function of the number of anchors for different strategies with $\sigma^2 = 100$ and $\sigma^2 = 20$. First, it can be observed that the SPEB decreases with the number of anchors for all strategies due to the diversity gain. Second, the optimal strategy, Strategy I, and Strategy II all outperform Uniform Strategy significantly, e.g., reducing the SPEB by more than 25% when $n = 10$. Third, the SPEB increases with the variance σ^2 of the prior knowledge. Moreover, the SPEBs of Strategy I and II are closer to that of the optimal strategy when σ^2 is smaller. This is because smaller variance σ^2 translates into more prior positional knowledge and thus, ranging measurements contribute less to the localization performance.

Case 3) Individual Resource Constraints: The performance of the optimal strategy, Strategy IV, and Strategy V are compared.

Consider that the upper bound of the individual resource follows an i.i.d. uniform distribution over different anchors, i.e., $x_k^{\max}$ is an instantiation of a random variable with uniform distribution from 0 and $\overline{P}$, $\forall k \in \mathcal{N}_b$, where $\overline{P}$ is a parameter to be selected. Fig. 14 shows the SPEB as a function of the
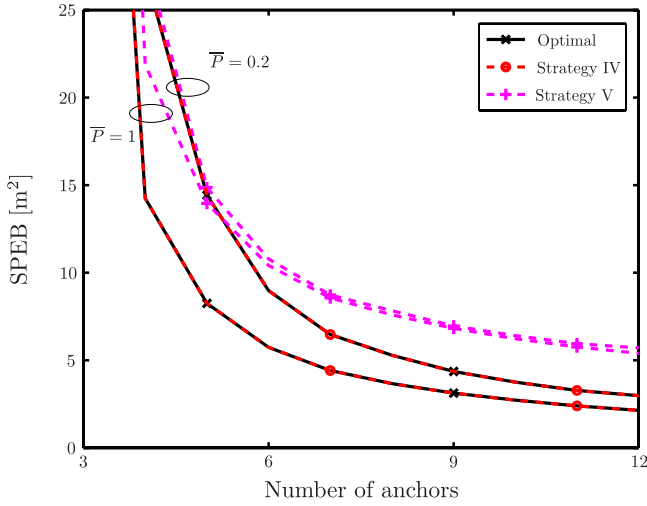
Fig. 14. Average SPEB as a function of the number of anchors for the optimal strategy, Strategy IV and Strategy V.

Fig. 15. Average SPEB as a function of $\overline{P}$ for the optimal strategy, Strategy IV and Strategy V.

number of anchors for different strategies with $\overline{P} = 0.2$ and 1. First, the SPEB decreases with the number of anchors due to the diversity gain. Second, Strategy IV and the optimal strategy provide almost the same performance, significantly outperforming Strategy V, e.g., reducing the SPEB by more than 40% when $n = 10$. Third, the SPEB decreases with $\overline{P}$ for the optimal strategy and Strategy IV because larger $\overline{P}$ implies a larger feasible set for the optimal strategy and Strategy IV, and therefore leads to smaller SPEB. Fourth, the SPEB achieved by Strategy V has almost the same value for $\overline{P} = 0.2$ and 1. This is because Strategy V usually allocates the resources evenly among anchors and hence individual resource constraints are often inactive, leading to almost the same performance of Strategy V for different values of $\overline{P}$.

Now consider that the upper bound of the individual resource is a constant for all anchors, i.e., $x_{\max}^k = \overline{P}$, $\forall k \in \mathcal{N}_b$. Fig. 15 shows the SPEB as a function of $\overline{P}$ for different strategies with $n = 10$ and 20. First, the SPEB decreases with $\overline{P}$ for both Strategy IV and the optimal strategy because larger $\overline{P}$ implies more relaxed individual constraints. This decreasing trend vanishes as $\overline{P}$ increases because the individual constraints are inactive for large $\overline{P}$. Second, it can be observed that Strategy V provides almost the same SPEB for different values of $\overline{P}$, similarly to Fig. 14. Third, Strategy IV and the optimal strategy provide almost the same performance, outperforming Strategy V significantly. Fourth, the SPEB for $n = 20$ is less than that for $n = 10$ due to the diversity gain.

Case 4) Robust Strategy: We denote $\Delta/100$ as the normalized uncertainty set size (NUSS), where the true position of the agent can be anywhere in the circle centered at its nominal position with radius Δ. Thus, the maximum uncertainty in d_k is Δ and in ϕ_k is $\arcsin(\Delta/d_k)$. The performance of non-robust strategy (the nominal values are used as the input), robust strategy proposed in Section VI-A, and Uniform Strategy are compared.

Fig. 16 and Fig. 17 show the worst-case SPEB and average SPEB as a function of the NUSS, respectively, with $n = 4$.
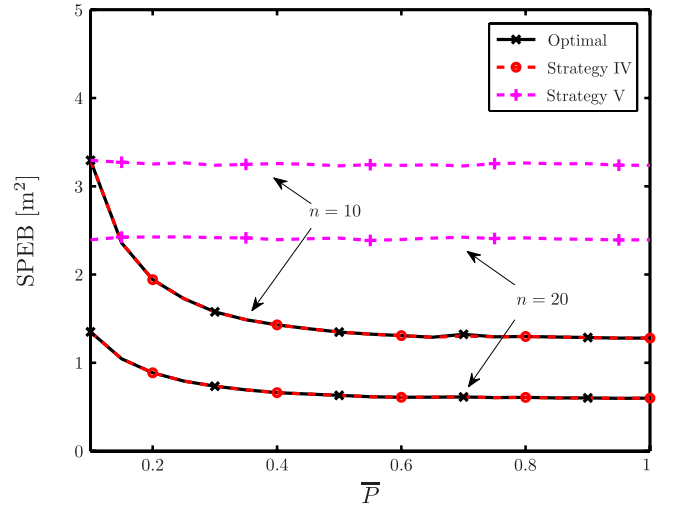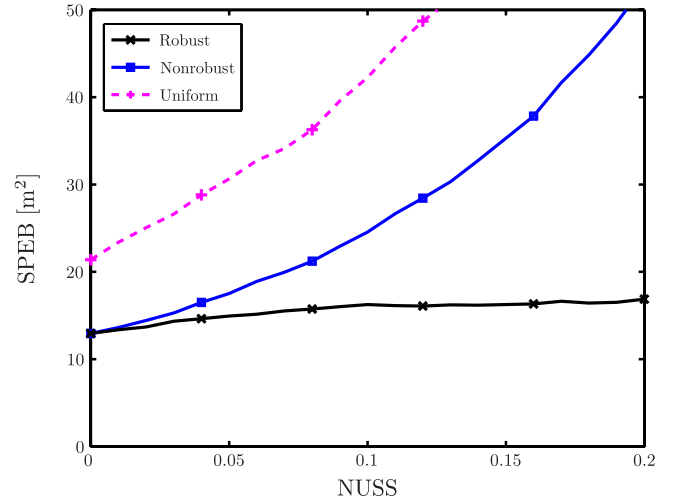
Fig. 16. Worst-case SPEB as a function of NUSS.

First, for the worst-case performance, the robust strategy outperforms Uniform Strategy and the non-robust strategy, particularly when NUSS is large. Second, the worst-case SPEBs achieved by all three strategies increase with the NUSS. This is because a larger NUSS translates to a larger range of possible network parameters and consequently a larger worst-case SPEB. Third, for the average performance, the robust strategy and the non-robust strategy have similar performances, both outperforming Uniform Strategy, especially when NUSS is small.

C. Efficiency of Geometric Methods

The efficiency of the proposed strategies is compared in this section under the same network setting as Section VII-B. The proposed strategies are run on a 2-GHz personal computer.

Case 1) Without Individual Constraints: Fig. 18 shows the running time as a function of the number of anchors for Strategy III, NPGM, and NPIV. First, the increasing speed differs for different strategies. This agrees with the computa-
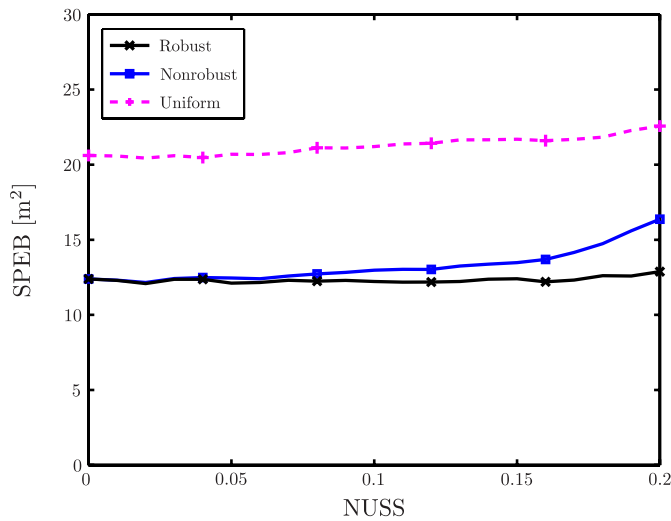
Fig. 17.   Average SPEB as a function of NUSS.

Fig. 19.   Running time as a function of the number of anchors for Strategy VI, Strategy IV and NPIC.

reducing the running time by more than 98% when $n = 15$. Second, the running time gap between Strategy VI and the other three strategies increases with the number of anchors. When $n > 7$, the linearity of the curve for Strategy VI shows that the computational complexity grows exponentially with n, which agrees with the analysis in Section V-A and shows that Strategy VI is impractical to implement. Third, Strategy IV has much less running time than the optimal strategy NPIC. Considering its near-optimal performance shown in Figs. 14 and 15, Strategy IV is a promising strategy since it achieves a good tradeoff between performance and complexity.
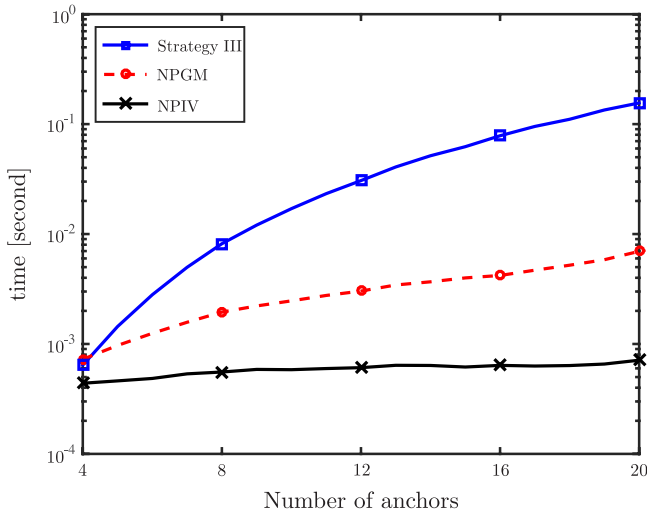

Fig. 18.   Running time as a function of the number of anchors for Strategy III, NPGM and NPIV.

tional complexity analysis in Section IV-D. Second, in terms of the running time, NPIV outperforms NPGM, and they both outperform Strategy III. Note that when n is large, NPIV and NPGM outperform Strategy III significantly (the running time is reduced by more than 90%). When n is small (e.g., $n < 10$), Strategy III is also efficient and may be adopted in practice since it is relatively easier for implementation. Third, the running time for NPIV almost remains a constant as n increases. This is because the running time of NPIV consists of two terms: $O(n \log h)$ for generating the convex hull and $O(h)$ for searching the set $\widetilde{\mathcal{K}}$. When n is small, the second term dominates the running time. Since h remains almost the same when n is small, as shown in Fig. 6, the running time for the second term does not increase and hence the total running time is almost a constant.

Case 2) With Individual Constraints: Fig. 19 shows the running time as a function of the number of anchors for NPIC, Strategy IV, and Strategy VI. First, Strategy IV and NPIC outperform Strategy VI significantly in the running time, e.g.,

VIII. CONCLUSION

This paper established a computational geometry framework to determine node prioritization strategies for efficient network localization. For node prioritization problems in the absence of individual constraints, we proved the sparsity property of the optimal NPV using geometric methods. We also designed efficient node prioritization strategies with complexity $O(n \log n)$. For node prioritization problems in the presence of individual constraints, we designed an efficient strategy with complexity $O(n^3 \log n)$ via the method of dimension augmentation and projection. Simulation results verified that the proposed approach provides significant improvement in localization accuracy and leads to reduction in computational complexity of the optimal NPV search. Our results provide a new methodology for node prioritization as well as insights into the optimization problems with similar structures.

APPENDIX I
APPLICATION OF THE NODE PRIORITIZATION PROBLEMS

We use wideband localization as an example to show the applications of the proposed method. Consider wideband waveforms transmitted from anchors to the agent as an

example. The waveform received at the agent is modeled as

$$r(t) = \sum_{k \in \mathcal{N}_{\mathrm{b}}} \frac{\sqrt{E_k}}{d_k^\beta} \sum_{l=1}^{L_k} \alpha_k^{(l)} s_k(t - \tau_k^{(l)}) + z_k(t)$$

where $d_k = \|\boldsymbol{p}_k - \boldsymbol{p}_0\|$, E_k is the transmission power of anchor k, β is the amplitude loss exponent, $\{s_k(t) : k \in \mathcal{N}_{\mathrm{b}}\}$ is a set of orthonormal transmission wideband waveforms, L_k is the number of multipath components associated with the channel from anchor k to the agent, $\alpha_k^{(l)}$ and $\tau_k^{(l)}$ are the path amplitude and delay of the l-th path, respectively, and $z_k(t)$ is the additive white complex Gaussian noise process with two-side power spectral density $N_0/2$. The path delay is given by

$$\tau_k^{(l)} = \frac{1}{c_{\mathrm{tr}}} \|\boldsymbol{p}_k - \boldsymbol{p}_0\| + b_k^{(l)}$$

where c_{tr} is the propagation speed of the transmission signal and $b_k^{(l)}$ is a range bias.

Starting from the received waveform $r(t)$, the fundamental limit of localization accuracy can be derived. The FIM is given by [10]

$$\boldsymbol{J}_{\mathrm{e}} = \boldsymbol{J}_0 + \sum_{k \in \mathcal{N}_{\mathrm{b}}} \varrho_k E_k \left(\int_{-\infty}^{+\infty} f^2 |S_k(f)|^2 df \right) \boldsymbol{J}_{\mathrm{r}}(\phi_k)$$

in which

$$\varrho_k = \frac{8\pi^2 |\alpha_k^{(1)}|^2 (1 - \chi_k)}{N_0 c_{\mathrm{tr}}^2 d_k^{2\beta}}$$

with $S_k(f)$ denoting the Fourier transform of $s_k(t)$ and $\chi_k \in [0,1]$ denoting the path-overlap coefficient. Next we show that node prioritization problems based on power and bandwidth can be converted to $\mathscr{P}$.

1) Node Prioritization based on Power: The node prioritization problem based on power is equivalent to $\mathscr{P}$ with $x_k = E_k$ and

$$\xi_k = \varrho_k \int_{-\infty}^{+\infty} f^2 |S_k(f)|^2 df.$$

2) Node Prioritization based on Bandwidth: Let $\mathcal{F}$ be the support of a given aggregated signal $S(f)$ in the frequency domain, and $\mathcal{F}_1$, $\mathcal{F}_2$, ..., $\mathcal{F}_n$ be a n−partition of $\mathcal{F}$ such that $\cup_{k \in \mathcal{N}_{\mathrm{b}}} \mathcal{F}_k = \mathcal{F}$ and $\mathcal{F}_k \cap \mathcal{F}_j = \varnothing$, $1 \le k \ne j \le n$. Node prioritization based on bandwidth is to find the n-partition of a given aggregate signal $S(f)$ so that the corresponding SPEB is minimized. Hence, the node prioritization problem based on bandwidth is equivalent to $\mathscr{P}$ with

$$x_k = \frac{\int_{\mathcal{F}_k} f^2 |S(f)|^2 df}{\int_{-\infty}^{+\infty} f^2 |S(f)|^2 df}$$

and $\xi_k = \varrho_k E_k$.

APPENDIX II
ALTERNATIVE PROOF OF THEOREM 2

The following lemma will be used in the proof.

Lemma 2: Given $n \in \mathbb{N}$ and $\boldsymbol{y}, \boldsymbol{z} \in \mathbb{R}^n$, if $\boldsymbol{y} \succ \boldsymbol{0}$ and $\boldsymbol{z} \ne \boldsymbol{0}$, there exists $\tilde{t} \in \mathbb{R}$ such that $\boldsymbol{y} + \tilde{t}\,\boldsymbol{z} \succeq \boldsymbol{0}$ and $\|\boldsymbol{y} + \tilde{t}\,\boldsymbol{z}\|_0 < n$.

Proof: This lemma can be proved by considering a mapping $\boldsymbol{f} : \mathbb{R} \to \mathbb{R}^n$

$$\boldsymbol{f}(t) = \boldsymbol{y} + t\,\boldsymbol{z}.$$

Note that (i) $\boldsymbol{f}(0) = \boldsymbol{y}$ is a vector with all positive elements; (ii) for sufficiently large M, if $t > M$, then either $\boldsymbol{f}(t)$ or $\boldsymbol{f}(-t)$ has at least one negative element; (iii) $\boldsymbol{f}(\cdot)$ is continuous on t. Thus, there exists $\tilde{t}$ such that $\boldsymbol{f}(\tilde{t}) \succeq \boldsymbol{0}$ with $\boldsymbol{f}(\tilde{t})$ containing at least one zero element, i.e., $\|\boldsymbol{f}(\tilde{t})\|_0 < n$. $\square$

Let $\boldsymbol{x}^*$ denote an optimal NPV for $\mathscr{P}_0$ with the minimum number of positive elements and let $m = \|\boldsymbol{x}^*\|_0$. If $m \le D$, the proof is completed. We next show that $m > D$ will lead to contradiction.

Without loss of generality, consider that the first m elements of $\boldsymbol{x}^*$ are positive, i.e.,

$$\boldsymbol{x}^* = [\,\boldsymbol{x}^{\mathrm{T}} \quad \boldsymbol{0}_{D-m}^{\mathrm{T}}\,]^{\mathrm{T}}.$$

Let $\boldsymbol{Q}(\boldsymbol{y})$ denote a function of $\boldsymbol{y} \in \mathbb{R}^m$

$$\boldsymbol{Q}(\boldsymbol{y}) = \boldsymbol{J}_0 + \sum_{k=1}^{m} y_k \, \boldsymbol{C}_k$$

where $\boldsymbol{C}_k = \xi_k \boldsymbol{u}_k \, \boldsymbol{u}_k^{\mathrm{T}}$ is a symmetric $d \times d$ matrix. Then $\boldsymbol{J}_{\mathrm{e}}(\boldsymbol{p}_0; \boldsymbol{x}^*)$ can be written as

$$\boldsymbol{J}_{\mathrm{e}}(\boldsymbol{p}_0; \boldsymbol{x}^*) = \boldsymbol{J}_0 + \sum_{k=1}^{m} x_k^* \boldsymbol{C}_k = \boldsymbol{Q}(\boldsymbol{x})$$

Let $[\boldsymbol{C}_k]_{ij} = c_k^l$ denote the elements of $\boldsymbol{C}_k$, where $l = \binom{j}{2} + i$ and let $\boldsymbol{c}_l = [\,c_1^l \quad c_2^l \quad \ldots \quad c_m^l\,]^{\mathrm{T}}$ for $l = 1, 2, \ldots, D$. The elements of $\boldsymbol{Q}(\boldsymbol{x})$ can then be written as

$$[\boldsymbol{Q}(\boldsymbol{x})]_{ij} = [\boldsymbol{J}_0]_{ij} + \sum_{k=1}^{m} x_k^* [\boldsymbol{C}_k]_{ij}$$
$$= [\boldsymbol{J}_0]_{ij} + \boldsymbol{x}^{\mathrm{T}} \boldsymbol{c}_l. \tag{19}$$

Since $\boldsymbol{c}_l \in \mathbb{R}^m$ and $m > D$, there exists a vector $\boldsymbol{g} \in \mathbb{R}^m$ orthogonal to $\{\,\boldsymbol{c}_l : l = 1, 2, \ldots, D\,\}$. Hence, for any $\eta \in \mathbb{R}$, $1 \le i, j \le d$,

$$[\boldsymbol{Q}(\boldsymbol{x} + \eta\,\boldsymbol{g})]_{ij} = [\boldsymbol{J}_0]_{ij} + (\boldsymbol{x} + \eta\,\boldsymbol{g})^{\mathrm{T}} \boldsymbol{c}_l = [\boldsymbol{Q}(\boldsymbol{x})]_{ij}$$

where the last equality is due to (19). This shows the invariance of FIM with respect to the NPV in the direction of $\boldsymbol{g}$. Next we show the contradiction for both cases $\boldsymbol{g}^{\mathrm{T}} \boldsymbol{1} \ne 0$ and $\boldsymbol{g}^{\mathrm{T}} \boldsymbol{1} = 0$, respectively.

If $\boldsymbol{g}^{\mathrm{T}} \boldsymbol{1} \ne 0$, choose ϵ such that the following two conditions hold: (i) $\epsilon \cdot \boldsymbol{g}^{\mathrm{T}} \boldsymbol{1} < 0$ and (ii) $\boldsymbol{x} + \epsilon \boldsymbol{g} \succ \boldsymbol{0}$. This is achievable since $\boldsymbol{x} \succ \boldsymbol{0}$, one can choose ϵ with $|\epsilon|$ sufficiently small. Let $\tilde{\boldsymbol{x}} = \boldsymbol{x} + \epsilon \boldsymbol{g}$ and $\tilde{\boldsymbol{x}}^* = [\,\tilde{\boldsymbol{x}}^{\mathrm{T}} \quad \boldsymbol{0}_{D-m}^{\mathrm{T}}\,]^{\mathrm{T}}$. Then

$$\boldsymbol{1}_n^{\mathrm{T}} \tilde{\boldsymbol{x}}^* = \boldsymbol{1}_m^{\mathrm{T}} \tilde{\boldsymbol{x}} < \boldsymbol{1}_m^{\mathrm{T}} \boldsymbol{x} = \boldsymbol{1}_n^{\mathrm{T}} \boldsymbol{x}^*.$$

Choose $\boldsymbol{y} = (\boldsymbol{1}_n^{\mathrm{T}} \boldsymbol{x}^* / \boldsymbol{1}_n^{\mathrm{T}} \tilde{\boldsymbol{x}}^*) \cdot \tilde{\boldsymbol{x}}^*$. One can verify that

$$\mathcal{P}(\boldsymbol{y}) \overset{(a)}{<} \mathcal{P}(\tilde{\boldsymbol{x}}^*) = \mathcal{P}(\boldsymbol{x}^*) \tag{20}$$

where (a) is due to the fact that $\boldsymbol{J}_{\mathrm{e}}(\boldsymbol{p}_0; \boldsymbol{y}) \succ \boldsymbol{J}_{\mathrm{e}}(\boldsymbol{p}_0; \tilde{\boldsymbol{x}}^*)$. Equation (20) implies that $\boldsymbol{y}$ outperforms $\boldsymbol{x}^*$, which contradicts the assumption that $\boldsymbol{x}^*$ is an optimal solution for $\mathscr{P}_0$.

If $\boldsymbol{g}^{\mathrm{T}} \mathbf{1} = 0$, consider $h(\eta) = \boldsymbol{x} + \eta \, \boldsymbol{g}$. By Lemma 2, there exists η_1 such that $h(\eta_1) \succeq \mathbf{0}$ and $\|h(\eta_1)\|_0 < m$. Consider vectors $\boldsymbol{x}' = h(\eta_1)$ and $\boldsymbol{x}'^* = [\, \boldsymbol{x}'^{\mathrm{T}} \;\; \mathbf{0}_{D-m}^{\mathrm{T}} \,]^{\mathrm{T}}$. Note that

- $\|\boldsymbol{x}'^*\|_0 = \|h(\eta_1)\|_0 < m = \|\boldsymbol{x}^*\|_0$;
- $\boldsymbol{J}_{\mathrm{e}}(\boldsymbol{p}_0; \boldsymbol{x}'^*) = \boldsymbol{Q}(\boldsymbol{x} + \eta_1 \boldsymbol{g}) = \boldsymbol{Q}(\boldsymbol{x}) = \boldsymbol{J}_{\mathrm{e}}(\boldsymbol{p}_0; \boldsymbol{x}^*)$ and hence $\mathcal{P}(\boldsymbol{x}'^*) = \mathcal{P}(\boldsymbol{x}^*)$; and
- $\mathbf{1}^{\mathrm{T}} \boldsymbol{x}'^* = \mathbf{1}^{\mathrm{T}} \boldsymbol{x} = \mathbf{1}^{\mathrm{T}} \boldsymbol{x}^*$.

This contradicts that $\boldsymbol{x}^*$ is an optimal NPV with the minimum number of positive elements.

APPENDIX III
PROOF OF PROPOSITION 7

The proof focuses on the case with $\boldsymbol{J}_0 = \mathbf{0}$ and the result is applicable to the case with any $\boldsymbol{J}_0 \succeq \mathbf{0}$. Let $\boldsymbol{x}^*$ denote an optimal solution for $\mathscr{P}_0$ with the minimum number of positive elements and let $m = \|\boldsymbol{x}^*\|_0$. We next show that $m > \mathrm{rank}\{\boldsymbol{\Lambda}\}$ will lead to contradiction.

Without loss of generality, consider that the first m elements in $\boldsymbol{x}^*$ are positive, i.e.,

$$\boldsymbol{x}^* = [\, \boldsymbol{x}^{\mathrm{T}} \;\; \mathbf{0}_{n-m}^{\mathrm{T}} \,]^{\mathrm{T}}. \tag{21}$$

Let $\widetilde{\boldsymbol{R}} = \mathrm{diag}\{\xi_1, \xi_2, \ldots, \xi_m\}$ and $\widetilde{\boldsymbol{\Lambda}}$ is the first principal $m \times m$ matrix of $\boldsymbol{\Lambda}$, i.e.,

$$\widetilde{\boldsymbol{\Lambda}} = \mathbf{1}\,\mathbf{1}^{\mathrm{T}} - \tilde{\boldsymbol{c}}\,\tilde{\boldsymbol{c}}^{\mathrm{T}} - \tilde{\boldsymbol{s}}\,\tilde{\boldsymbol{s}}^{\mathrm{T}}$$

with

$$\tilde{\boldsymbol{c}} = [\, \cos\phi_1 \;\; \cos\phi_2 \;\; \ldots \;\; \cos\phi_m \,]^{\mathrm{T}}$$
$$\tilde{\boldsymbol{s}} = [\, \sin\phi_1 \;\; \sin\phi_2 \;\; \ldots \;\; \sin\phi_m \,]^{\mathrm{T}}.$$

Lemma 3: If $\boldsymbol{y} = \boldsymbol{x} + \left(\boldsymbol{I} - \widetilde{\boldsymbol{R}}^{-1} \widetilde{\boldsymbol{\Lambda}}^{+} \widetilde{\boldsymbol{\Lambda}} \widetilde{\boldsymbol{R}} \right) \boldsymbol{w}$, where $\boldsymbol{x}$ is the vector consisting of the first m elements of $\boldsymbol{x}^*$ in (21), and $\boldsymbol{w}$ is an arbitrary real vector satisfying $\boldsymbol{y} \succeq \mathbf{0}$, then

$$\boldsymbol{y}^* = [\, \boldsymbol{y}^{\mathrm{T}} \;\; \mathbf{0}_{n-m}^{\mathrm{T}} \,]^{\mathrm{T}}$$

is an optimal NPV for $\mathscr{P}_0$.

Proof: To prove $\boldsymbol{y}^*$ is an optimal NPV for $\mathscr{P}_0$, it suffices to prove that $\boldsymbol{y}^*$ achieves the same SPEB as $\boldsymbol{x}^*$ and that $\boldsymbol{x}^*$ satisfies the total resource constraint.

One can verify that $\mathrm{span}\{\mathbf{1}, \tilde{\boldsymbol{c}}, \tilde{\boldsymbol{s}}\} = \mathrm{span}\{\text{columns of } \widetilde{\boldsymbol{\Lambda}}\}$ and hence $\mathbf{1}^{\mathrm{T}}(\boldsymbol{I} - \widetilde{\boldsymbol{\Lambda}}^{+} \widetilde{\boldsymbol{\Lambda}}) = \mathbf{0}^{\mathrm{T}}$. Consequently,

$$\mathbf{1}^{\mathrm{T}} \widetilde{\boldsymbol{R}} \left(\boldsymbol{I} - \widetilde{\boldsymbol{R}}^{-1} \widetilde{\boldsymbol{\Lambda}}^{+} \widetilde{\boldsymbol{\Lambda}} \widetilde{\boldsymbol{R}} \right) = \mathbf{0}^{\mathrm{T}} \tag{22}$$

Note that

$$\mathbf{1}_n^{\mathrm{T}} \boldsymbol{R} \boldsymbol{x}^* \overset{(a)}{=} \mathbf{1}_m^{\mathrm{T}} \widetilde{\boldsymbol{R}} \boldsymbol{x} \overset{(b)}{=} \mathbf{1}_m^{\mathrm{T}} \widetilde{\boldsymbol{R}} \boldsymbol{y} \overset{(c)}{=} \mathbf{1}_n^{\mathrm{T}} \boldsymbol{R} \boldsymbol{y}^* \tag{23}$$

where (a) is due to the relationship between $\boldsymbol{x}^*$ and $\boldsymbol{x}$, (b) is due to (22), and (c) is due to the relationship between $\boldsymbol{y}$ and $\boldsymbol{y}^*$.

The definition of Moore-Penrose pseudo-inverse gives $\widetilde{\boldsymbol{\Lambda}}(\boldsymbol{I} - \widetilde{\boldsymbol{\Lambda}}^{+}) \widetilde{\boldsymbol{\Lambda}} = \mathbf{0}$. Consequently,

$$\widetilde{\boldsymbol{R}} \widetilde{\boldsymbol{\Lambda}} \widetilde{\boldsymbol{R}} \left(\boldsymbol{I} - \widetilde{\boldsymbol{R}}^{-1} \widetilde{\boldsymbol{\Lambda}}^{+} \widetilde{\boldsymbol{\Lambda}} \widetilde{\boldsymbol{R}} \right) = \mathbf{0}. \tag{24}$$

Note that

$$\boldsymbol{x}^{*\mathrm{T}} \boldsymbol{R} \boldsymbol{\Lambda} \boldsymbol{R} \boldsymbol{x}^* \overset{(d)}{=} \boldsymbol{x}^{\mathrm{T}} \widetilde{\boldsymbol{R}} \widetilde{\boldsymbol{\Lambda}} \widetilde{\boldsymbol{R}} \boldsymbol{x} \overset{(e)}{=} \boldsymbol{y}^{\mathrm{T}} \widetilde{\boldsymbol{R}} \widetilde{\boldsymbol{\Lambda}} \widetilde{\boldsymbol{R}} \boldsymbol{y} \overset{(f)}{=} \boldsymbol{y}^{*\mathrm{T}} \boldsymbol{R} \boldsymbol{\Lambda} \boldsymbol{R} \boldsymbol{y}^* \tag{25}$$

where (d) is due to (21), (e) is due to (24), and (f) is due to the relationship between $\boldsymbol{y}$ and $\boldsymbol{y}^*$. Equations (23) and (25) imply that $\mathcal{P}(\boldsymbol{x}^*) = \mathcal{P}(\boldsymbol{y}^*)$. As with the analysis in Appendix II, $\mathbf{1}^{\mathrm{T}} \boldsymbol{x} \neq \mathbf{1}^{\mathrm{T}} \boldsymbol{y}$ leads to a contradiction. Therefore,

$$\mathbf{1}^{\mathrm{T}} \boldsymbol{x}^* = \mathbf{1}^{\mathrm{T}} \boldsymbol{x} = \mathbf{1}^{\mathrm{T}} \boldsymbol{y} = \mathbf{1}^{\mathrm{T}} \boldsymbol{y}^*$$

indicating that $\boldsymbol{y}^*$ satisfies the total resource constraint and hence the proof is completed. $\qquad \square$

With Lemma 3, we can prove Proposition 7 by showing that $m > \mathrm{rank}\{\boldsymbol{\Lambda}\}$ will lead to contradiction. Note that $m > \mathrm{rank}\{\boldsymbol{\Lambda}\} \geq \mathrm{rank}\{\widetilde{\boldsymbol{\Lambda}}\}$, which gives $\boldsymbol{I} - \widetilde{\boldsymbol{\Lambda}}^{+} \widetilde{\boldsymbol{\Lambda}} \neq \mathbf{0}$, and equivalently, $\left(\boldsymbol{I} - \widetilde{\boldsymbol{R}}^{-1} \widetilde{\boldsymbol{\Lambda}}^{+} \widetilde{\boldsymbol{\Lambda}} \widetilde{\boldsymbol{R}} \right) \neq \mathbf{0}$. Suppose its lth column is not $\mathbf{0}$. Consider the following mapping

$$h(t) = \boldsymbol{x} + \left(\boldsymbol{I} - \widetilde{\boldsymbol{R}}^{-1} \widetilde{\boldsymbol{\Lambda}}^{+} \widetilde{\boldsymbol{\Lambda}} \widetilde{\boldsymbol{R}} \right) \boldsymbol{e}_l \cdot t$$

where $\boldsymbol{e}_l \in \mathbb{R}^m$. Lemma 2 implies that there exists t_1 such that (i) $h(t_1) \succeq \mathbf{0}$ and (ii) $\|h(t_1)\|_0 < m$. Consider

$$\tilde{\boldsymbol{x}} = [\, h(t_1)^{\mathrm{T}} \;\; \mathbf{0}^{\mathrm{T}} \,]^{\mathrm{T}}.$$

By Lemma 3, $\tilde{\boldsymbol{x}}$ is an optimal NPV for $\mathscr{P}_0$ and $\|\tilde{\boldsymbol{x}}\|_0 < m$. This contradicts the assumption that $\boldsymbol{x}^*$ is an optimal NPV with the minimum number of positive elements.

APPENDIX IV
ALGEBRAIC METHOD FOR OPTIMAL STRATEGY IN SIMPLE NETWORKS

We first present the solution of $\mathscr{P}_0$ with $\boldsymbol{J}_0 = \mathbf{0}$ in simple networks and then propose a prior knowledge decomposition method to solve $\mathscr{P}_0$ with $\boldsymbol{J}_0 \neq \mathbf{0}$ in simple networks.

A. Solving $\mathscr{P}_0$ With No Prior Knowledge in Simple Networks

Note that when $\boldsymbol{J}_0 = \mathbf{0}$, the SPEB is

$$\mathcal{P}(\boldsymbol{x}) = \frac{4 \cdot \mathbf{1}^{\mathrm{T}} \boldsymbol{R} \boldsymbol{x}}{\boldsymbol{x}^{\mathrm{T}} \boldsymbol{R}^{\mathrm{T}} \boldsymbol{\Lambda} \boldsymbol{R} \boldsymbol{x}} =: \widetilde{\mathcal{P}}(\boldsymbol{x}).$$

The proposition provides an efficient method to check if the minimum number of active anchors is three, and if so, then it provides the optimal NPV for $\mathscr{P}_0$ analytically.

Proposition 14: If the following conditions hold

$$\mathrm{rank}\{\boldsymbol{\Lambda}\} = 3 \tag{26a}$$
$$\mathbf{1}^{\mathrm{T}} (\boldsymbol{R} \boldsymbol{\Lambda} \boldsymbol{R})^{-1} \mathbf{1} > 0 \tag{26b}$$
$$(\boldsymbol{R} \boldsymbol{\Lambda} \boldsymbol{R})^{-1} (\boldsymbol{R} \mathbf{1} + c \, \mathbf{1}) \succ \mathbf{0} \tag{26c}$$

where

$$c = \sqrt{1/(\mathbf{1}^{\mathrm{T}} (\boldsymbol{R} \boldsymbol{\Lambda} \boldsymbol{R})^{-1} \mathbf{1})} \tag{27}$$

then there exists a unique optimal NPV for $\mathscr{P}_0$, given by

$$\boldsymbol{x}^* = \frac{A}{2c} (\boldsymbol{R} \boldsymbol{\Lambda} \boldsymbol{R})^{-1} (\boldsymbol{R} \mathbf{1} + c \, \mathbf{1}) \tag{28}$$

where

$$A = \frac{2c}{\mathbf{1}^{\mathrm{T}} (\boldsymbol{R} \boldsymbol{\Lambda} \boldsymbol{R})^{-1} (\boldsymbol{R} \mathbf{1} + c \mathbf{1})} \tag{29}$$

and the corresponding SPEB is

$$\mathcal{P}(\boldsymbol{x}^*) = 2 \cdot \mathbf{1}^{\mathrm{T}} (\boldsymbol{R}\boldsymbol{\Lambda}\boldsymbol{R})^{-1} (\boldsymbol{R}\mathbf{1} + c\mathbf{1}).$$

Otherwise, there exists an optimal NPV for $\mathscr{P}_0$ with at most two positive elements.

Proof: See Appendix V. □

The closed-form strategy for $\mathscr{P}_0$ in simple networks is given as follows. Let $s : \mathcal{N}_{\mathrm{b}} \times \mathcal{N}_{\mathrm{b}} \to \mathbb{R}$ denote the function

$$s(i, j) = \frac{(1/\sqrt{\xi_i} + 1/\sqrt{\xi_j})^2}{\sin^2(\phi_i - \phi_j)}$$

in which $i, j \in \mathcal{N}_{\mathrm{b}}$ and $\sin(\phi_i - \phi_j) \neq 0$. Two strategies are provided as follows.

- π_1: the optimal solution is given by (28);
- π_2: let $(k_1, k_2) = \arg\min_{\{i,j\}} s(i, j)$ and k_3 is the remaining anchor, the NPV is

$$x_{k_1} = \frac{\sqrt{\xi_{k_2}}}{\sqrt{\xi_{k_1}} + \sqrt{\xi_{k_2}}}, \quad x_{k_2} = \frac{\sqrt{\xi_{k_1}}}{\sqrt{\xi_{k_1}} + \sqrt{\xi_{k_2}}}, \quad x_{k_3} = 0.$$

Proposition 15: For a simple network with $\boldsymbol{J}_0 = \boldsymbol{0}$, if the conditions in (26) hold, the optimal node prioritization strategy $\pi^* = \pi_1$, otherwise $\pi^* = \pi_2$. Moreover, the SPEB is given by

$$\mathcal{P}(\boldsymbol{x}^*) = \begin{cases} \frac{4c}{A} & \text{if } \pi^* = \pi_1 \\ \min_{\{i,j\}} s(i, j) & \text{if } \pi^* = \pi_2. \end{cases}$$

Proof: If conditions in (26) hold, π_1 is an optimal strategy by the proof of Proposition 14. Otherwise, there exists an optimal strategy that requires two active anchors. Suppose anchors i and j are active, then

$$\begin{aligned}
\mathcal{P}(\boldsymbol{x}) &= \frac{x_i \xi_i + x_j \xi_j}{x_i x_j \, \xi_i \xi_j \sin^2(\phi_i - \phi_j)} \\
&= \frac{1}{\sin^2(\phi_i - \phi_j)} \Big(\frac{1}{\xi_i x_i} + \frac{1}{\xi_j x_j}\Big) \\
&= \frac{x_i + x_j}{\sin^2(\phi_i - \phi_j)} \Big(\frac{1}{\xi_i x_i} + \frac{1}{\xi_j x_j}\Big) \\
&\geq s(i, j).
\end{aligned}$$

The last inequality is due to Cauchy-Schwarz inequality and the equality holds iff $x_i = x_j \sqrt{\xi_j/\xi_i}$. Minimizing $s(i, j)$ over i, j leads to $(i^*, j^*) = \arg\min_{\{i,j\}} s(i, j)$ and thus anchors i^* and j^* are active. □

B. Solving $\mathscr{P}_0$ With Prior Knowledge in Simple Networks

Although the problem $\mathscr{P}_0$ for simple networks can be obtained by checking the KKT conditions, we propose the following method, referred to as *prior knowledge decomposition*, to solve $\mathscr{P}_0$ with much simpler derivations.

Lemma 4 (Prior Knowledge Decomposition): For an arbitrary symmetric $\boldsymbol{J}_0$ and a simple network, rank$\{\boldsymbol{\Lambda}\} = 3$ implies rank$\{\boldsymbol{\Lambda}_{\mathrm{e}}\} = 3$, where

$$\boldsymbol{\Lambda}_{\mathrm{e}} = \boldsymbol{P}\,[\,\mathbf{1} \quad \boldsymbol{c} \quad \boldsymbol{s}\,]^{\mathrm{T}}\,\boldsymbol{R}$$

in which

$$\boldsymbol{P} = \begin{bmatrix} 1/2 & 1/2 & 0 \\ 0 & 0 & 1/2 \\ 1/2 & -1/2 & 0 \end{bmatrix}.$$

Moreover, if rank$\{\boldsymbol{\Lambda}_{\mathrm{e}}\} = 3$, then the vector

$$\boldsymbol{x}_0 = \boldsymbol{\Lambda}_{\mathrm{e}}^{-1}\,[\,[\boldsymbol{J}_0]_{11}\,[\boldsymbol{J}_0]_{12}\,[\boldsymbol{J}_0]_{22}\,]^{\mathrm{T}}$$

satisfies that

$$\boldsymbol{J}_0 = \sum_{k \in \mathcal{N}_{\mathrm{b}}} [\boldsymbol{x}_0]_k \, \xi_k \, \boldsymbol{J}_{\mathrm{r}}(\phi_k). \tag{30}$$

Proof: If rank$\{\boldsymbol{\Lambda}\} = 3$, then $\mathbf{1}$, $\boldsymbol{c}$ and $\boldsymbol{s}$ are linearly independent. Note that both $\boldsymbol{P}$ and $\boldsymbol{R}$ are invertible. Hence rank$\{\boldsymbol{\Lambda}_{\mathrm{e}}\} = 3$.

The second claim can be verified after some algebra. □

Lemma 4 shows that if rank$\{\boldsymbol{\Lambda}\} = 3$, the prior positional knowledge can be viewed as localization information obtained by allocating certain (possibly negative) resources to the existing anchors.

If rank$\{\boldsymbol{\Lambda}\} = 3$, $\boldsymbol{J}_0$ can be decomposed as (30). Let

$$\tilde{\boldsymbol{x}} = \boldsymbol{x} + \boldsymbol{x}_0$$

then the SPEB with prior positional knowledge is given by

$$\mathcal{P}(\boldsymbol{x}) = \widetilde{\mathcal{P}}(\tilde{\boldsymbol{x}}) = \frac{4 \cdot \mathbf{1}^{\mathrm{T}} \boldsymbol{R} \tilde{\boldsymbol{x}}}{\tilde{\boldsymbol{x}}^{\mathrm{T}} \boldsymbol{R}^{\mathrm{T}} \boldsymbol{\Lambda} \boldsymbol{R} \tilde{\boldsymbol{x}}}.$$

Consider an ancillary node prioritization problem:

$$\widetilde{\mathscr{P}}_0 : \; \underset{\tilde{\boldsymbol{x}} \in \mathbb{R}^3}{\text{minimize}} \quad \widetilde{\mathcal{P}}(\tilde{\boldsymbol{x}})$$
$$\text{subject to} \quad \mathbf{1}^{\mathrm{T}} \tilde{\boldsymbol{x}} \leq 1 + \mathbf{1}^{\mathrm{T}} \boldsymbol{x}_0$$
$$\tilde{\boldsymbol{x}} \succeq \boldsymbol{x}_0.$$

If $\tilde{\boldsymbol{x}}^*$ is an optimal NPV for $\widetilde{\mathscr{P}}_0$, then $\boldsymbol{x}^* = \tilde{\boldsymbol{x}}^* - \boldsymbol{x}_0$ is an optimal NPV for $\mathscr{P}_0$. The objective function of $\widetilde{\mathscr{P}}_0$ has a simple expression. Therefore, previous results for $\boldsymbol{J}_0 = \boldsymbol{0}$ can be used to derive the solution for $\widetilde{\mathscr{P}}_0$.

Proposition 16: If the following conditions hold

$$\text{rank}\{\boldsymbol{\Lambda}\} = 3 \tag{31a}$$
$$\mathbf{1}^{\mathrm{T}} (\boldsymbol{R}\boldsymbol{\Lambda}\boldsymbol{R})^{-1} \mathbf{1} > 0 \tag{31b}$$
$$A(\boldsymbol{R}\boldsymbol{\Lambda}\boldsymbol{R})^{-1}(\boldsymbol{R}\mathbf{1} + c\mathbf{1}) \succ \frac{2c}{(1 + \mathbf{1}^{\mathrm{T}} \boldsymbol{x}_0)} \boldsymbol{x}_0 \tag{31c}$$

where c, A, and $\boldsymbol{x}_0$ are repectively given by (27), (29), and (30), then there exists a unique optimal NPV for $\mathscr{P}_0$, given by

$$\boldsymbol{x}^* = \frac{A\,(1 + \mathbf{1}^{\mathrm{T}} \boldsymbol{x}_0)}{2c} (\boldsymbol{R}\boldsymbol{\Lambda}\boldsymbol{R})^{-1}(\boldsymbol{R}\mathbf{1} + c\mathbf{1}) - \boldsymbol{x}_0 \tag{32}$$

and the corresponding SPEB is

$$\mathcal{P}(\boldsymbol{x}^*) = 2 \cdot \mathbf{1}^{\mathrm{T}} (\boldsymbol{R}\boldsymbol{\Lambda}\boldsymbol{R})^{-1}(\boldsymbol{R}\mathbf{1} + c\mathbf{1})/(1 + \mathbf{1}^{\mathrm{T}} \boldsymbol{x}_0).$$

Otherwise, there exists an optimal solution for $\mathscr{P}_0$ with at most two positive elements.

Proof: If the conditions in (31) hold, one can decompose $\boldsymbol{J}_0$ and obtain $\boldsymbol{x}_0$ in (30). For problem $\widetilde{\mathscr{P}}_0$, similar to the derivation in Appendix V, one can verify that there exists a unique optimal NPV $\tilde{\boldsymbol{x}}^*$ for $\widetilde{\mathscr{P}}_0$, given by

$$\tilde{\boldsymbol{x}}^* = \frac{A\,(1 + \boldsymbol{1}^{\mathrm{T}}\boldsymbol{x}_0)}{2c}\,(\boldsymbol{R}\boldsymbol{\Lambda}\boldsymbol{R})^{-1}(\boldsymbol{R}\boldsymbol{1} + c\,\boldsymbol{1}).$$

Therefore, $\boldsymbol{x}^* = \tilde{\boldsymbol{x}}^* - \boldsymbol{x}_0$ is the unique optimal NPV for $\mathscr{P}_0$. If the conditions in (31) do not hold, then either $\mathrm{rank}\{\boldsymbol{\Lambda}\} = 3$ or $\mathrm{rank}\{\boldsymbol{\Lambda}\} \leq 2$. For the former, one can decompose $\boldsymbol{J}_0$ and verify that there exists an optimal NPV for $\mathscr{P}_0$ with at most two positive elements using the similar derivation in Appendix V; for the latter, the proof is completed by Proposition 7. □

Next we present the case where at most two anchors are required to achieve the minimum SPEB for $\mathscr{P}_0$.

Proposition 17: For a network with three anchors (i.e., $\mathcal{N}_{\mathrm{b}} = \{1, 2, 3\}$) where the conditions in (31) do not hold, if there exist $\boldsymbol{x}$ and i, j, k such that

$$C_j \xi_i - C_i \xi_j - E_{i,j} = (2x_j^2 \xi_i \xi_j^2 - 2x_i^2 \xi_i^2 \xi_j)\sin^2(\phi_i - \phi_j) \tag{33}$$

$$x_i + x_j = 1, \ x_i > 0, \ x_j > 0, \ x_k = 0 \tag{34}$$

$$\frac{\partial}{\partial x_i}\mathcal{P}(\boldsymbol{x}) < \frac{\partial}{\partial x_k}\mathcal{P}(\boldsymbol{x}) \tag{35}$$

where

$$C_i = 2\xi_i\left(\mathrm{tr}\{\boldsymbol{J}_0\} + ([\boldsymbol{J}_0]_{22} - [\boldsymbol{J}_0]_{11})\cos\phi_i + 4[\boldsymbol{J}_0]_{12}\sin\phi_i\right)$$
$$E_{i,j} = \mathrm{tr}\{\boldsymbol{J}_0\}\left(2\xi_i\xi_j(x_j - x_i)\sin^2(\phi_i - \phi_j) + C_i - C_j\right)$$

then the optimal NPV for $\mathscr{P}_0$ is given by $\boldsymbol{x}$. Otherwise, there exists an optimal NPV for $\mathscr{P}_0$ with only one non-zero element.

The proof of Proposition 17 is obtained by checking the KKT conditions. Combining (33) and (34) gives a quadratic equation of x_i and this equation can be solved analytically to achieve $\boldsymbol{x}$; then one can check whether the inequality (35) holds.

The optimal NPV for $\mathscr{P}_0$ in simple networks is provided as follows:

- Conditions (31) hold: the optimal NPV $\boldsymbol{x}^*$ is given by (32);
- Conditions (31) do not hold:
  - if there exists $\boldsymbol{x}$ such that (33) to (35) hold, then NPV $\boldsymbol{x}^* = \boldsymbol{x}$;
  - Otherwise, the optimal NPV for $\mathscr{P}_0$ has one non-zero element and can be obtained by checking three anchors one by one.

APPENDIX V
PROOF OF PROPOSITION 14

The NPV $\boldsymbol{x}^*$ is an optimal solution for $\mathscr{P}_0$ iff it satisfies KKT conditions

$$\begin{cases} \nabla\mathcal{P}(\boldsymbol{x}^*) - \boldsymbol{\mu} + \nu \cdot \nabla(\boldsymbol{1}^{\mathrm{T}}\boldsymbol{x}^* - 1) = \boldsymbol{0} \\ \boldsymbol{x}^* \succeq \boldsymbol{0}, \ \boldsymbol{\mu} \succeq \boldsymbol{0}, \ \mu_k x_k^* = 0, \ k = 1, 2, 3 \\ \boldsymbol{1}^{\mathrm{T}}\boldsymbol{x}^* = 1 \end{cases}$$

If conditions (26) hold, one can verify that the NPV provided in (28) satisfies the KKT conditions above with $\boldsymbol{\mu} = \boldsymbol{0}$. The uniqueness is shown as follows. Suppose there exists another optimal NPV $\tilde{\boldsymbol{x}}^*$ for $\mathscr{P}_0$; then $\|\tilde{\boldsymbol{x}}^*\|_0 = 3$ or $\|\tilde{\boldsymbol{x}}^*\|_0 \leq 2$.

If $\|\tilde{\boldsymbol{x}}^*\|_0 = 3$, then $\mu_j = 0$, $j = 1, 2, 3$. Checking KKT conditions with respect to $\tilde{\boldsymbol{x}}^*$, one can obtain

$$\tilde{\boldsymbol{x}}^* = \frac{A}{2c}\,(\boldsymbol{R}\boldsymbol{\Lambda}\boldsymbol{R})^{-1}(\boldsymbol{R}\boldsymbol{1} + c\,\boldsymbol{1}) \tag{36}$$

where $A = \tilde{\boldsymbol{x}}^{*\mathrm{T}}\boldsymbol{R}\boldsymbol{\Lambda}\boldsymbol{R}\tilde{\boldsymbol{x}}^*$ and $c = (\boldsymbol{R}\boldsymbol{1})^{\mathrm{T}}\tilde{\boldsymbol{x}}^*$. Substituting (36) into $\boldsymbol{1}^{\mathrm{T}}\tilde{\boldsymbol{x}}^* = 1$ and the fact that

$$(\boldsymbol{R}\boldsymbol{1})^{\mathrm{T}}(\boldsymbol{R}\boldsymbol{\Lambda}\boldsymbol{R})^{-1}\boldsymbol{R}\boldsymbol{1} = 1$$

give (27) and (29). Consequently, $\tilde{\boldsymbol{x}}^*$ in (36) is identical to $\boldsymbol{x}^*$ in (28). Moreover, by substituting $\tilde{\boldsymbol{x}}^*$ into $\mathcal{P}(\cdot)$, one can show that $\mathcal{P}(\boldsymbol{x}^*) = 2 \cdot \boldsymbol{1}^{\mathrm{T}}(\boldsymbol{R}\boldsymbol{\Lambda}\boldsymbol{R})^{-1}(\boldsymbol{R}\boldsymbol{1} + c\boldsymbol{1})$.

If $\|\tilde{\boldsymbol{x}}^*\|_0 \leq 2$, consider a linear combination of $\boldsymbol{x}^*$ and $\tilde{\boldsymbol{x}}^*$ with respect to $\delta \in (0, 1)$: $\boldsymbol{x}_\delta = (1 - \delta)\boldsymbol{x}^* + \delta\tilde{\boldsymbol{x}}^*$. Note that $\|\boldsymbol{x}_\delta\|_0 = 3$. By the convexity of $\mathcal{P}(\cdot)$, $\boldsymbol{x}_\delta$ is also an optimal NPV. This statement contradicts that $\boldsymbol{x}^*$ is a unique NPV with three positive elements. Hence, $\boldsymbol{x}^*$ is the unique optimal NPV if the conditions in (26) hold.

On the other hand, if the conditions in (26) do not hold, we claim that there exists an optimal NPV for $\mathscr{P}_0$ with at most two positive elements. Otherwise, the optimal NPV $\boldsymbol{x}^*$ for $\mathscr{P}_0$ has three positive elements. If there are more than one optimal NPV, each of them has three positive elements. Then by Lemma 7, $\mathrm{rank}\{\boldsymbol{\Lambda}\} = 3$ and therefore $\mathrm{rank}\{\boldsymbol{R}\boldsymbol{\Lambda}\boldsymbol{R}\} = 3$. KKT conditions imply $\boldsymbol{x}^* = A\,(\boldsymbol{R}\boldsymbol{\Lambda}\boldsymbol{R})^{-1}(\boldsymbol{R}\boldsymbol{1} + c\,\boldsymbol{1})/(2c)$. Since c is a real number, $\boldsymbol{1}^{\mathrm{T}}(\boldsymbol{R}\boldsymbol{\Lambda}\boldsymbol{R})^{-1}\boldsymbol{1} > 0$. Moreover, since $A/2c = 2/\mathcal{P}(\boldsymbol{x}) > 0$, $\boldsymbol{x}^* \succ \boldsymbol{0}$ implies

$$(\boldsymbol{R}\boldsymbol{\Lambda}\boldsymbol{R})^{-1}(\boldsymbol{R}\boldsymbol{1} + c\,\boldsymbol{1}) \succ \boldsymbol{0}.$$

Then all conditions in (26) hold, which contradicts the assumption that the conditions in (26) do not hold.

APPENDIX VI
PROOF OF PROPOSITION 10

The proof can be divided into two cases that depend on the position of $\boldsymbol{y}^*$ relative to $\mathcal{Y}$: (i) $\boldsymbol{y}^*$ is an interior point of a face f^* of $\mathcal{Y}$ and (ii) $\boldsymbol{y}^*$ lies in an edge of $\mathcal{Y}$. The proof focuses on the first case and the result can be easily extended to the second case.

The following lemma can be used for checking the visibility of a face.

Lemma 5: Given a facet $\tilde{f}$ of a convex polyhedron $\mathcal{C}$ and a point p. $\tilde{f}$ is visible from p iff $\langle \boldsymbol{n}, \boldsymbol{h}\rangle < 0$, where $\boldsymbol{n}$ denotes the outward-pointing normal vector of $\tilde{f}$ and $\boldsymbol{h}$ is a vector from p to an arbitrary point in $\tilde{f}$.

Lemma 5 can be verified directly from the Definition 1. Let $\boldsymbol{h}^* = [y_1^*, y_2^*, y_3^* - \mu]^{\mathrm{T}}$ denote the vector from $\boldsymbol{y}_\mu$ to $\boldsymbol{y}^*$. Since $\boldsymbol{y}^*$ is an interior point of f^*, normal vectors of f^* and that of the hyperboloid (8) are aligned at $\boldsymbol{y}^*$, implying that the outward-pointing normal vector of f^* can be written as

$$\boldsymbol{n}^* = t\,[-y_1^*, -y_2^*, y_3^* - 2/\lambda^*]^{\mathrm{T}}$$

where $\lambda^* = \mathcal{P}(\boldsymbol{x}^*) > 0$ and t is a nonzero constant. Note that $-\boldsymbol{n}^*$, the outward-pointing normal vector of (8), satisfies that $-n_3^* \leq 0$, implying that

$$t(y_3^* - 2/\lambda^*) \geq 0. \tag{37}$$

Moreover, note that $y_3 = \boldsymbol{1}^{\mathrm{T}} \boldsymbol{R} \boldsymbol{x} + \mathrm{tr}\{\boldsymbol{J}_0\} > 0$ and

$$(y_3^* - 2/\lambda^*)^2 = y_1^{*2} + y_2^{*2} + 4(\lambda^*)^{-2} \geq 4(\lambda^*)^{-2}$$

which gives

$$y_3^* \geq 4/\lambda^*. \tag{38}$$

Together with (37), this shows that $t > 0$. Without loss of generality, we consider $t = 1$. Then the inner product of $\boldsymbol{n}^*$ and $\boldsymbol{h}^*$ is

$$\langle \boldsymbol{n}^*, \boldsymbol{h}^* \rangle = -y_1^{*2} - y_2^{*2} + y_3^{*2} - \mu y_3^* - 2y_3^*/\lambda^* + 2\mu/\lambda^*$$
$$\overset{(a)}{=} \mu(2/\lambda^* - y_3^*) + 2y_3^*/\lambda^*$$

where (a) is because $\boldsymbol{y}^*$ is on the curve (8). Note that

$$y_3^* > 2/\lambda^* > 0$$

according to (38). Hence, $\mu(2/\lambda^* - y_3^*) > 0$ and $2y_3^*/\lambda^* > 0$. Consequently, $\langle \boldsymbol{n}^*, \boldsymbol{h}^* \rangle > 0$ and, by Lemma 5, f is not visible from the point $\boldsymbol{y}_\mu$.

APPENDIX VII
PROOF OF THE CLAIM IN SECTION V

The following lemma shows that $\mathcal{Y}_{\mathrm{B}}$ is a translate of $\widetilde{\mathcal{Y}}_{\mathrm{B}}$.

Lemma 6: There exists a constant $\boldsymbol{d}$ such that $\mathcal{Y}_{\mathrm{B}} = \widetilde{\mathcal{Y}}_{\mathrm{B}} + \boldsymbol{d}$.

Proof: This lemma can be proved by induction. For $N = 2$, $\mathcal{Y}_{\mathrm{B}}$ obtained by Line 1 to Line 3 in Algorithm 4 is a parallelogram, and its edges (in a clockwise order) are either $(\boldsymbol{y}_1, \boldsymbol{y}_2, -\boldsymbol{y}_1, -\boldsymbol{y}_2)$ or $(\boldsymbol{y}_1, -\boldsymbol{y}_2, -\boldsymbol{y}_1, \boldsymbol{y}_2)$, depending on the angles of $\boldsymbol{y}_1$ and $\boldsymbol{y}_2$. In either case, there exists a constant $\boldsymbol{d}^{(2)}$ such that $\mathcal{Y}_{\mathrm{B}} = \widetilde{\mathcal{Y}}_{\mathrm{B}} + \boldsymbol{d}^{(2)}$.

Let

$$\mathcal{Y}_{\mathrm{B}}^{(i)} = \left\{ \sum_{k=1}^{i} c_k \boldsymbol{y}_k : 0 \leq c_k \leq 1 \right\}$$

and let $\widetilde{\mathcal{Y}}_{\mathrm{B}}^{(i)}$ denote the polygon obtained by Line 1 to Line 3 in Algorithm 4 with input vectors $\boldsymbol{y}_1, \boldsymbol{y}_2, \ldots, \boldsymbol{y}_i$. Note that $\mathcal{Y}_{\mathrm{B}} = \mathcal{Y}_{\mathrm{B}}^{(N)}$ and $\widetilde{\mathcal{Y}}_{\mathrm{B}} = \widetilde{\mathcal{Y}}_{\mathrm{B}}^{(N)}$.

Suppose the lemma is proved for $N = l - 1$. The induction hypothesis implies that there exists a constant $\boldsymbol{d}^{(l-1)}$ such that $\mathcal{Y}_{\mathrm{B}}^{(l-1)} = \widetilde{\mathcal{Y}}_{\mathrm{B}}^{(l-1)} + \boldsymbol{d}^{(l-1)}$. Consider the case $N = l$. Note that

$$\mathcal{Y}_{\mathrm{B}}^{(l)} = \left\{ \boldsymbol{y} : \boldsymbol{y} = t \cdot \boldsymbol{y}_l + \boldsymbol{z}, \boldsymbol{z} \in \mathcal{Y}_{\mathrm{B}}^{(l-1)}, 0 \leq t \leq 1 \right\} \tag{39}$$

and

$$\widetilde{\mathcal{Y}}_{\mathrm{B}}^{(l)} = \left\{ \boldsymbol{y} : \boldsymbol{y} = t \cdot \boldsymbol{y}_l + \widetilde{\boldsymbol{z}} + \boldsymbol{r}, \widetilde{\boldsymbol{z}} \in \widetilde{\mathcal{Y}}_{\mathrm{B}}^{(l-1)}, 0 \leq t \leq 1 \right\} \tag{40}$$

for some constant $\boldsymbol{r}$ that depends on $\boldsymbol{y}_l$ and $\widetilde{\mathcal{Y}}_{\mathrm{B}}^{(l-1)}$. Comparing (39) and (40) shows that $\mathcal{Y}_{\mathrm{B}}^{(l)} = \widetilde{\mathcal{Y}}_{\mathrm{B}}^{(l)} + \boldsymbol{d}^{(l)}$, where $\boldsymbol{d}^{(l)}$ is given by $\boldsymbol{d}^{(l)} = \boldsymbol{d}^{(l-1)} - \boldsymbol{r}$. $\square$

Next consider the point in $\mathcal{Y}_{\mathrm{B}}$ with the largest x-component, denoted as $\boldsymbol{y}_{\mathrm{r}}$. This point is unique since none of the

vectors $\boldsymbol{y}_1, \boldsymbol{y}_2, \ldots, \boldsymbol{y}_N$ is parallel to the vertical axis. Therefore, together with Lemma 6, $\mathcal{Y}_{\mathrm{B}}$ can be obtained by translating $\widetilde{\mathcal{Y}}_{\mathrm{B}}$ so that $\widetilde{\boldsymbol{y}}_{\mathrm{R}}$ overlaps $\boldsymbol{y}_{\mathrm{r}}$. The only thing remaining to show is that $\boldsymbol{y}_{\mathrm{r}}$ is identical to the point $\boldsymbol{y}_{\mathrm{R}}$ obtained in Line 4 and Line 5. Let $X(\boldsymbol{y})$ denote the x-component of a two-dimensional vector $\boldsymbol{y}$. Then

$$
\begin{aligned}
\boldsymbol{y}_{\mathrm{r}} &= \arg\max_{\boldsymbol{y} \in \mathcal{Y}_{\mathrm{B}}} X(\boldsymbol{y}) \\
&= \arg\max_{\boldsymbol{y} = \sum_{i=1}^{N} c_i \boldsymbol{y}_i, 0 \leq c_i \leq 1} X(\boldsymbol{y}) \\
&= \arg\max_{\boldsymbol{y} = \sum c_i \boldsymbol{y}_i, 0 \leq c_i \leq 1, X(\boldsymbol{y}_i) \geq 0} X(\boldsymbol{y}) \\
&= \sum_{X(\boldsymbol{y}_i) \geq 0} \boldsymbol{y}_i \\
&= \boldsymbol{y}_{\mathrm{R}}.
\end{aligned}
$$

REFERENCES

[1] M. Z. Win *et al.*, "Network localization and navigation via cooperation," *IEEE Commun. Mag.*, vol. 49, no. 5, pp. 56–62, May 2011.

[2] U. A. Khan, S. Kar, and J. M. F. Moura, "Distributed sensor localization in random environments using minimal number of anchor nodes," *IEEE Trans. Signal Process.*, vol. 57, no. 5, pp. 2000–2016, May 2009.

[3] Y. Shen, S. Mazuelas, and M. Z. Win, "Network navigation: Theory and interpretation," *IEEE J. Sel. Areas Commun.*, vol. 30, no. 9, pp. 1823–1834, Oct. 2012.

[4] K. Plarre and P. R. Kumar, "Tracking objects with networked scattered directional sensors," *EURASIP J. Adv. Signal Process.*, vol. 2008, Dec. 2007, Art. no. 360912.

[5] U. A. Khan, S. Kar, and J. M. F. Moura, "DILAND: An algorithm for distributed sensor localization with noisy distance measurements," *IEEE Trans. Signal Process.*, vol. 58, no. 3, pp. 1940–1947, Mar. 2010.

[6] B. Denis, J.-B. Pierrot, and C. Abou-Rjeily, "Joint distributed synchronization and positioning in UWB ad hoc networks using TOA," *IEEE Trans. Microw. Theory Techn.*, vol. 54, no. 4, pp. 1896–1911, Jun. 2006.

[7] A. Rabbachin, I. Oppermann, and B. Denis, "GML ToA estimation based on low complexity UWB energy detection," in *Proc. IEEE Int. Symp. Pers., Indoor Mobile Radio Commun.*, Helsinki, Finland, Sep. 2006, pp. 1–5.

[8] S. Gezici *et al.*, "Localization via ultra-wideband radios: A look at positioning aspects for future sensor networks," *IEEE Signal Process. Mag.*, vol. 22, no. 4, pp. 70–84, Jul. 2005.

[9] A. H. Sayed, A. Tarighat, and N. Khajehnouri, "Network-based wireless location: Challenges faced in developing techniques for accurate wireless location information," *IEEE Signal Process. Mag.*, vol. 22, no. 4, pp. 24–40, Jul. 2005.

[10] Y. Shen and M. Z. Win, "Fundamental limits of wideband localization— Part I: A general framework," *IEEE Trans. Inf. Theory*, vol. 56, no. 10, pp. 4956–4980, Oct. 2010.

[11] J. J. Caffery and G. L. Stüber, "Overview of radiolocation in CDMA cellular systems," *IEEE Commun. Mag.*, vol. 36, no. 4, pp. 38–45, Apr. 1998.

[12] C.-Y. Chong and S. P. Kumar, "Sensor networks: Evolution, opportunities, and challenges," *Proc. IEEE*, vol. 91, no. 8, pp. 1247–1256, Aug. 2003.

[13] K. Pahlavan, X. Li, and J.-P. Mäkelä, "Indoor geolocation science and technology," *IEEE Commun. Mag.*, vol. 40, no. 2, pp. 112–118, Feb. 2002.

[14] H. Godrich, A. M. Haimovich, and R. S. Blum, "Target localization accuracy gain in MIMO radar-based systems," *IEEE Trans. Inf. Theory*, vol. 56, no. 6, pp. 2783–2803, Jun. 2010.

[15] A. M. Haimovich, R. S. Blum, and L. J. Cimini, "MIMO radar with widely separated antennas," *IEEE Signal Process. Mag.*, vol. 25, no. 1, pp. 116–129, Jan. 2008.

[16] E. Paolini, A. Giorgetti, M. Chiani, R. Minutolo, and M. Montanari, "Localization capability of cooperative anti-intruder radar systems," *EURASIP J. Adv. Signal Process.*, vol. 2008, p. 726854, Dec. 2008.

[17] L. Mailaender, "On the geolocation bounds for round-trip time-of-arrival and all non-line-of-sight channels," *EURASIP J. Adv. Signal Process.*, vol. 2008, Jan. 2008, Art. no. 37.

[18] Y. Shen, H. Wymeersch, and M. Z. Win, "Fundamental limits of wideband localization—Part II: Cooperative networks," *IEEE Trans. Inf. Theory*, vol. 56, no. 10, pp. 4981–5000, Oct. 2010.

[19] D. Jourdan, D. Dardari, and M. Win, "Position error bound for UWB localization in dense cluttered environments," *IEEE Trans. Aerosp. Electron. Syst.*, vol. 44, no. 2, pp. 613–628, Apr. 2008.

[20] Y. Qi, H. Kobayashi, and H. Suda, "Analysis of wireless geolocation in a non-line-of-sight environment," *IEEE Trans. Wireless Commun.*, vol. 5, no. 3, pp. 672–681, Mar. 2006.

[21] F. Meshkati, H. V. Poor, and S. C. Schwartz, "Energy-efficient resource allocation in wireless networks," *IEEE Signal Process. Mag.*, vol. 24, no. 3, pp. 58–68, May 2007.

[22] M. Gorlatova, P. Kinget, I. Kymissis, D. Rubenstein, X. Wang, and G. Zussman, "Energy harvesting active networked tags (EnHANTs) for ubiquitous object networking," *IEEE Wireless Commun. Mag.*, vol. 17, no. 6, pp. 18–25, Dec. 2010.

[23] F. P. Kelly, A. K. Maulloo, and D. K. H. Tan, "Rate control for communication networks: Shadow prices, proportional fairness and stability," *J. Oper. Res. Soc.*, vol. 49, no. 3, pp. 237–252, Mar. 1998.

[24] Z.-Q. Luo and W. Yu, "An introduction to convex optimization for communications and signal processing," *IEEE J. Sel. Areas Commun.*, vol. 24, no. 8, pp. 1426–1438, Aug. 2006.

[25] G. J. Foschini, "Private conversation," AT&T Labs-Res., Middletown, NJ, USA, Tech. Rep., May 2001.

[26] L. A. Shepp, "Private conversation," AT&T Labs-Res., Middletown, NJ, USA, Tech. Rep., Mar. 2001.

[27] W. Dai, Y. Shen, and M. Z. Win, "On the minimum number of active anchors for optimal localization," in *Proc. IEEE Global Telecommun. Conf.*, Anaheim, CA, USA, Dec. 2012, pp. 4951–4956.

[28] W. Dai, Y. Shen, and M. Z. Win, "Sparsity-inspired power allocation for network localization," in *Proc. IEEE Int. Conf. Commun.*, Budapest, Hungary, Jun. 2013, pp. 2785–2790.

[29] Y. Shen, W. Dai, and M. Z. Win, "Power optimization for network localization," *IEEE/ACM Trans. Netw.*, vol. 22, no. 4, pp. 1337–1350, Aug. 2014.

[30] Y. Shen and M. Z. Win, "Energy efficient location-aware networks," in *Proc. IEEE Int. Conf. Commun.*, Beijing, China, May 2008, pp. 2995–3001.

[31] H. Godrich, A. P. Petropulu, and H. V. Poor, "Power allocation strategies for target localization in distributed multiple-radar architectures," *IEEE Trans. Signal Process.*, vol. 59, no. 7, pp. 3226–3240, Jul. 2011.

[32] W. W.-L. Li, Y. Shen, Y. J. Zhang, and M. Z. Win, "Robust power allocation for energy-efficient location-aware networks," *IEEE/ACM Trans. Netw.*, vol. 21, no. 6, pp. 1918–1930, Dec. 2013.

[33] T. Wang, G. Leus, and L. Huang, "Ranging energy optimization for robust sensor positioning based on semidefinite programming," *IEEE Trans. Signal Process.*, vol. 57, no. 12, pp. 4777–4787, Dec. 2009.

[34] M. Grant and S. Boyd. (Aug. 2010). *CVX: MATLAB Software for Disciplined Convex Programming, Version 1.21*. [Online]. Available: http://cvxr.com/cvx

[35] D. Peaucelle, D. Henrion, and Y. Labit. (Nov. 2001). *User's Guide for SeDuMi Interface 1.01*. [Online]. Available: http://www.optimization-online.org/DB_HTML/2001/11/398.html

[36] D. Dardari, A. Conti, U. Ferner, A. Giorgetti, and M. Z. Win, "Ranging with ultrawide bandwidth signals in multipath environments," *Proc. IEEE*, vol. 97, no. 2, pp. 404–426, Feb. 2009.

[37] H. L. Van Trees, K. L. Bell, and Z. Tian, *Detection Estimation and Modulation Theory, Part I: Detection, Estimation, and Filtering Theory*. New York, NY, USA: Wiley, 1968.

[38] H. V. Poor, *An Introduction to Signal Detection and Estimation*, 2nd ed. New York, NY, USA: Springer-Verlag, 1994.

[39] W. Dai, Y. Shen, and M. Z. Win, "Energy-efficient network navigation algorithms," *IEEE J. Sel. Areas Commun.*, vol. 33, no. 7, pp. 1418–1430, Jul. 2015.

[40] S. Boyd and L. Vandenberghe, *Convex Optimization*. Cambridge, U.K.: Cambridge Univ. Press, 2004.

[41] T. M. Chan, "Optimal output-sensitive convex hull algorithms in two and three dimensions," *Discrete Comput. Geometry*, vol. 16, no. 4, pp. 361–368, 1996.

[42] M. de Berg, O. Cheong, M. van Kreveld, and M. Overmars, *Computational Geometry: Algorithms and Applications*. Berlin, Germany: Springer-Verlag, 2008.

[43] M. S. Lobo, L. Vandenberghe, S. Boyd, and H. Lebret, "Applications of second-order cone programming," *Linear Algebra Appl.*, vol. 284, nos. 1–3, pp. 193–228, Nov. 1998.

[44] J. D. Gorman and A. O. Hero, "Lower bounds for parametric estimation with constraints," *IEEE Trans. Inf. Theory*, vol. 26, no. 6, pp. 1285–1301, Nov. 1990.

[45] *Technical Specification LTE; Evolved Universal Terrestrial Radio Access (E-UTRA); User Equipment (UE) Radio Transmission and Reception*, document 3GPP TS 136.101 V11.2.0 (2012-11) Release 11, 3rd Generation Partnership Project, Nov. 2012.

Wenhan Dai (S'12) received the B.S. degrees in Electronic Engineering and in Mathematics from Tsinghua University in 2011, and the S.M. degree in Aeronautics and Astronautics at the Massachusetts Institute of Technology (MIT) in 2014.

He is pursuing the Ph.D. degree with Wireless Information and Network Sciences Laboratory at MIT. His research interests include communication theory and stochastic optimization with application to wireless communication and network localization. His current research focuses on efficient network localization, cooperative network operation, and ultra-wideband communication.

Mr. Dai was honored by the Marconi Society with the Paul Baran Young Scholar Award (2017). He received the Marconi-BISITE Best Paper Award from the IEEE ICUWB (2017), the Chinese Government Award for Outstanding Student Abroad (2016), the first prize of the IEEE Communications Society Student Competition (2016), and the Student Paper Award (first place) from the IEEE CWIT (2015). He was recognized as the exemplary reviewer of the IEEE COMMUNICATIONS LETTERS (2014).

Yuan Shen (S'05–M'14) received the Ph.D. degree and the S.M. degree in electrical engineering and computer science from the Massachusetts Institute of Technology (MIT), Cambridge, MA, USA, in 2014 and 2008, respectively, and the B.E. degree (with highest honor) in electronic engineering from Tsinghua University, Beijing, China, in 2005.

He is an Associate Professor with the Department of Electronic Engineering at Tsinghua University. Prior to that, he was a Research Assistant and then Postdoctoral Associate with the Wireless Information and Network Sciences Laboratory at MIT in 2005-2014. He was with the Hewlett-Packard Labs in winter 2009 and the Corporate R&D at Qualcomm Inc. in summer 2008. His research interests include statistical inference, network science, communication theory, information theory, and optimization. His current research focuses on network localization and navigation, inference techniques, resource allocation, and intrinsic wireless secrecy.

Professor Shen was a recipient of the Qiu Shi Outstanding Young Scholar Award (2015), the China's Youth 1000-Talent Program (2014), the Marconi Society Paul Baran Young Scholar Award (2010), and the MIT Walter A. Rosenblith Presidential Fellowship (2005). His papers received the IEEE Communications Society Fred W. Ellersick Prize (2012) and three Best Paper Awards from the IEEE Globecom (2011), ICUWB (2011), and WCNC (2007). He is elected Vice Chair (2017-2018) and Secretary (2015-2016) for the IEEE ComSoc Radio Communications Committee. He serves as TPC symposium Co-Chair for the IEEE Globecom (2016), the European Signal Processing Conference (EUSIPCO) (2016), and the IEEE ICC Advanced Network Localization and Navigation (ANLN) Workshop (2016 and 2017). He also serves as Editor for the IEEE COMMUNICATIONS LETTERS since 2015 and Guest-Editor for the *International Journal of Distributed Sensor Networks* (2015).

Moe Z. Win (S'85–M'87–SM'97–F'04) is a professor at the Massachusetts Institute of Technology (MIT) and the founding director of the Wireless Information and Network Sciences Laboratory. Prior to joining MIT, he was with AT&T Research Laboratories and NASA Jet Propulsion Laboratory.

His research encompasses fundamental theories, algorithm design, and network experimentation for a broad range of real-world problems. His current research topics include network localization and navigation, network interference exploitation, and quantum information science. He has served the IEEE Communications Society as an elected Member-at-Large on the Board of Governors, as elected Chair of the Radio Communications Committee, and as an IEEE Distinguished Lecturer. Over the last two decades, he held various Editorial posts for IEEE journals and organized numerous international conferences. Currently, he is serving on the SIAM Diversity Advisory Committee.

Dr. Win is an elected Fellow of the AAAS, the IEEE, and the IET. He was honored with two IEEE Technical Field Awards: the IEEE Kiyo Tomiyasu Award (2011) and the IEEE Eric E. Sumner Award (2006, jointly with R. A. Scholtz). Together with students and colleagues, his papers have received numerous awards. Other recognitions include the IEEE Communications Society Edwin H. Armstrong Achievement Award (2016), the International Prize for Communications Cristoforo Colombo (2013), the Copernicus Fellowship (2011) and the *Laurea Honoris Causa* (2008) from the University of Ferrara, and the U.S. Presidential Early Career Award for Scientists and Engineers (2004). He is an ISI Highly Cited Researcher.